Energy dependence of transverse momentum fluctuations in Pb+Pb collisions at the CERN Super Proton Synchrotron (SPS) at 20A to 158A GeV

The NA49 Collaboration

Abstract

Results are presented on event-by-event fluctuations of transverse momenta p_T in central Pb+Pb interactions at 20A, 30A, 40A, 80A, and 158A GeV. The analysis was performed for charged particles at forward center-of-mass rapidity ($1.1 < y^*_\pi < 2.6$). Three fluctuation measures were studied: the distribution of average transverse momentum - $M(p_T)$ - in the event, the Φ_{p_T} fluctuation measure and two-particle transverse momentum correlations. Fluctuations of p_T are small and show no significant energy dependence in the energy range of the CERN Super Proton Synchrotron. Results are compared with QCD-inspired predictions for the critical point, and with the UrQMD model. Transverse momentum fluctuations, similar to multiplicity fluctuations, do not show the increase expected for freeze-out near the critical point of QCD.

The NA49 Collaboration

T. Anticic[23], B. Baatar[8],D. Barna[4], J. Bartke[6], L. Betev[10], H. Białkowska[20], C. Blume[9], B. Boimska[20], M. Botje[1], J. Bracinik[3], P. Bunčić[10], V. Cerny[3], P. Christakoglou[2], P. Chung[19], O. Chvala[14], J.G. Cramer[16], P. Csató[4], P. Dinkelaker[9], V. Eckardt[13], Z. Fodor[4], P. Foka[7], V. Friese[7], J. Gál[4], M. Gaździcki[9,11], V. Genchev[18], E. Gładysz[6], K. Grebieszkow[22], S. Hegyi[4], C. Höhne[7], K. Kadija[23], A. Karev[13], D. Kikola[22], V.I. Kolesnikov[8], E. Kornas[6], R. Korus[11], M. Kowalski[6], M. Kreps[3], A. Laszlo[4], R. Lacey[19], M. van Leeuwen[1], P. Lévai[4], L. Litov[17], B. Lungwitz[9], M. Makariev[17], A.I. Malakhov[8], M. Mateev[17], G.L. Melkumov[8], A. Mischke[1], M. Mitrovski[9], J. Molnár[4], St. Mrówczyński[11], V. Nicolic[23], G. Pálla[4], A.D. Panagiotou[2], D. Panayotov[17], A. Petridis[2,*], W. Peryt[22], M. Pikna[3], J. Pluta[22], D. Prindle[16], F. Pühlhofer[12], R. Renfordt[9], C. Roland[5], G. Roland[5], M. Rybczyński[11], A. Rybicki[6], A. Sandoval[7], N. Schmitz[13], T. Schuster[9], P. Seyboth[13], F. Siklér[4], B. Sitar[3], E. Skrzypczak[21], M. Slodkowski[22], G. Stefanek[11], R. Stock[9], C. Strabel[9], H. Ströbele[9], T. Susa[23], I. Szentpétery[4], J. Sziklai[4], M. Szuba[22], P. Szymanski[10,20], V. Trubnikov[20], M. Utvic[9], D. Varga[4,10], M. Vassiliou[2], G.I. Veres[4,5], G. Vesztergombi[4], D. Vranić[7], Z. Włodarczyk[11], A. Wojtaszek[11], I.K. Yoo[15]

[1]NIKHEF, Amsterdam, Netherlands.
[2]Department of Physics, University of Athens, Athens, Greece.
[3]Comenius University, Bratislava, Slovakia.
[4]KFKI Research Institute for Particle and Nuclear Physics, Budapest, Hungary.
[5]MIT, Cambridge, USA.
[6]Institute of Nuclear Physics, Cracow, Poland.
[7]Gesellschaft für Schwerionenforschung (GSI), Darmstadt, Germany.
[8]Joint Institute for Nuclear Research, Dubna, Russia.
[9]Fachbereich Physik der Universität, Frankfurt, Germany.
[10]CERN, Geneva, Switzerland.
[11]Institute of Physics, Jan Kochanowski University, Kielce, Poland.
[12]Fachbereich Physik der Universität, Marburg, Germany.
[13]Max-Planck-Institut für Physik, Munich, Germany.
[14]Institute of Particle and Nuclear Physics, Charles University, Prague, Czech Republic.
[15]Department of Physics, Pusan National University, Pusan, Republic of Korea.
[16]Nuclear Physics Laboratory, University of Washington, Seattle, WA, USA.
[17]Atomic Physics Department, Sofia University St. Kliment Ohridski, Sofia, Bulgaria.
[18]Institute for Nuclear Research and Nuclear Energy, Sofia, Bulgaria.
[19]Department of Chemistry, Stony Brook Univ. (SUNYSB), Stony Brook, USA.
[20]Institute for Nuclear Studies, Warsaw, Poland.
[21]Institute for Experimental Physics, University of Warsaw, Warsaw, Poland.
[22]Faculty of Physics, Warsaw University of Technology, Warsaw, Poland.
[23]Rudjer Boskovic Institute, Zagreb, Croatia.
[*]deceased

1 Introduction and Motivation

For more than 30 years, experiments studying relativistic nucleus-nucleus ($A + A$) collisions have been carried out in laboratories in Europe and the United States. The main motivation has been to test the hypothesis that strongly interacting matter at energy densities exceeding about 1 GeV/fm^3 exists in the form of deconfined quarks and gluons, eventually forming the quark-gluon plasma (QGP) [1]. Recent results from the CERN Super Proton Synchrotron (SPS) and BNL Relativistic Heavy Ion Collider (RHIC) seem to confirm this conjecture. The data suggest that the threshold for the onset of deconfinement is located at the low SPS energies [2, 3].

The phase diagram of strongly interacting matter can be presented in terms of temperature T and baryochemical potential μ_B. QCD-inspired calculations suggest that the phase boundary between hadrons and QGP is of first order at large values of μ_B, ending in a critical point of second order and then turning into a continuous rapid transition at low μ_B [4]. The location of the critical point may be close to the (T, μ_B) values found for the freeze-out of the hadron system produced in collisions of heavy nuclei at SPS energies.

The study of fluctuations is an important tool for localizing the phase boundary and the critical point. In particular, significant transverse momentum and multiplicity fluctuations are expected to appear for systems that hadronize from QGP and freeze-out near the critical point of QCD [5]. The location of the freeze-out point in the phase diagram can be moved by varying the collision energy and the size of the collision system. A nonmonotonic evolution of fluctuations with these collision parameters can serve as a signature for the phase transition and the critical point. These considerations motivated an extensive program of fluctuation studies at the SPS and RHIC accelerators.

So far for central Pb+Pb collisions, the analysis of multiplicity fluctuations has found only small effects without significant structure in the energy dependence in the whole SPS energy domain [6]. The measured net charge fluctuations can be explained by the effects of global charge conservation [7]. The energy dependence of event-by-event fluctuations of the K/π ratio, on the other hand, shows an interesting increase toward lower energies [8] that can be attributed to the onset of deconfinement [9] rather than to the critical point.

This paper presents results of the NA49 experiment from a study of transverse momentum p_T fluctuations in central Pb+Pb collisions at $20A$, $30A$, $40A$, $80A$, and $158A$ GeV. It extends a previous study [10] that investigated the system size dependence of p_T fluctuations at the top SPS energy.

Fluctuations in nucleus-nucleus collisions are susceptible to two trivial sources: the finite and fluctuating number of produced particles and event-by-event fluctuations of the collision geometry (see the discussion of this point within HSD and UrQMD transport models in Ref. [11]). Suitable statistical tools have to be chosen to extract the fluctuations of interest. As in the previous NA49 study [10], mainly the global Φ_{p_T} measure will be used. Alternative measures used in the literature, e.g. $\sigma_{p_T,dyn}$ [12], $\Delta\sigma_{p_T}$ [13], F_{p_T} [14], and $\Sigma_{p_T}(\%)$ [15, 16] are related [17].

To obtain further information on the possible source of fluctuations, two additional methods will be employed. The distribution of event-wise average transverse momentum $M(p_T)$ will be compared against the corresponding histogram for mixed events, which represents purely statistical fluctuations. Moreover, two-particle transverse momentum correlations, as proposed in Ref. [13], will be analyzed.

This paper is organized as follows. In Sec. 2 the statistical tools used in this analysis are introduced and briefly discussed. The NA49 setup is presented in Sec. 3. Experimen-

tal effects such as detector acceptance and two-track resolution are discussed in Sec. 4. The NA49 results on the energy dependence of transverse momentum fluctuations are presented and discussed in Sec. 5. A summary closes the paper.

2 Measures of fluctuations

Various methods can be used to measure event-by-event p_T fluctuations. A natural observable is the distribution of the average transverse momentum of the events defined as

$$M(p_T) = \frac{1}{N}\sum_{i=1}^{N} p_{Ti}, \tag{1}$$

where N is the multiplicity of accepted particles in a given event and p_{Ti} is the transverse momentum of the i-th particle. The distribution of $M(p_T)$ will be compared with the corresponding histogram obtained for artificially produced "mixed events". In mixed events, all particles are by construction uncorrelated (each particle in a given mixed event is taken from a different real event with the same multiplicity) but follow the experimental inclusive three-momentum spectra as well as the distribution of multiplicity.

The second observable used in this work is the Φ_{p_T} measure, proposed in Ref. [18] and used also in our previous analysis [10]. Following the authors of Ref. [18], one can define the single-particle variable $z_{p_T} = p_T - \overline{p_T}$ with the bar denoting averaging over the single-particle inclusive distribution. As seen, $\overline{z_{p_T}} = 0$. Further, one introduces the event variable Z_{p_T}, which is a multiparticle analog of z_{p_T}, defined as

$$Z_{p_T} = \sum_{i=1}^{N}(p_{Ti} - \overline{p_T}), \tag{2}$$

where the summation runs over particles in a given event. Note, that $\langle Z_{p_T}\rangle = 0$, where $\langle ...\rangle$ represents averaging over events. Finally, the Φ_{p_T} measure is defined as

$$\Phi_{p_T} = \sqrt{\frac{\langle Z_{p_T}^2\rangle}{\langle N\rangle}} - \sqrt{\overline{z_{p_T}^2}}. \tag{3}$$

The Φ_{p_T} measure has two important properties. First, Φ_{p_T} vanishes when the system consists of particles that are emitted independently (no interparticle correlations), and the single particle momentum spectrum is independent of multiplicity. Second, if an $A + A$ collision can be treated as an incoherent superposition of independent $N + N$ interactions (superposition model), then Φ_{p_T} has a constant value, the same for $A + A$ and $N + N$ interactions. This implies that, in particular, Φ_{p_T} does not depend on the impact parameter (centrality), if the $A + A$ collision is a simple superposition of $N + N$ interactions. Furthermore, Φ_{p_T} is independent of changes of the size of a compact acceptance domain provided the correlation scale (range), l_C, is much smaller than the size of the acceptance region, l_A. In the limit of large correlation length and small acceptance the magnitude of Φ_{p_T} is proportional to the multiplicity of accepted particles. Thus for a small acceptance Φ_{p_T} approaches zero. The approximately linear dependence of Φ_{p_T} on the fraction of accepted particles in the limit $l_A \ll l_C$ suggested the introduction of the fluctuation measures $\Sigma_{p_T}(\%)$ [16] and $\sigma_{p_T,dyn}$ [12], which for large particle multiplicities are proportional to $\sqrt{\Phi_{p_T}/\langle N\rangle}$. These properties of the fluctuation measures should be

taken into account when results are compared and discussed. Finally, we note that the magnitude of Φ_{p_T} decreases with the fraction of randomly lost particles, e.g., due to incomplete reconstruction efficiency.

In spite of the above mentioned advantages, there is an important disadvantage of using Φ_{p_T} in the fluctuation analysis. While Φ_{p_T} is sensitive to the presence of particle correlations in a system, it does not provide information on the nature of the correlation. Several effects can contribute to Φ_{p_T}. Therefore, to achieve a better understanding of the fluctuation structure, it is useful to also employ a more differential method [13].

The correlations can be studied by plotting the cumulative p_T variables for particle pairs. Namely, instead of p_T, one can introduce the variable x, defined for a particle i as [19]

$$x(p_T) = \int_0^{p_T} \rho(p_T{}')dp_T{}', \tag{4}$$

where $\rho(p_T)$ is the inclusive p_T distribution, normalized to unity, which is obtained from all particles used in the analysis. By construction, the x variable varies between 0 and 1 with a *flat* probability distribution. Two-particle correlation plots, as presented in this paper, are obtained by plotting (x_1, x_2) points for all possible particle pairs within the same event. The number of pairs in each (x_1, x_2) bin is divided by the mean number of pairs in a bin (averaged over all (x_1, x_2) bins). This two-dimensional plot is *uniformly* populated when no interparticle correlations are present in the system. Nonuniformity signals the presence of interparticle correlations. For example, when identical particles are studied, Bose statistics lead to a ridge along the diagonal of the (x_1, x_2) plot, which starts at $(0, 0)$ and ends at $(1, 1)$, whereas event-by-event temperature fluctuations produce a saddle-shaped structure [13].

3 Experimental Setup

NA49 is one of the fixed target experiments at the CERN SPS. The detector (see Fig. 1 and Ref. [20]) is a large acceptance hadron spectrometer used for the study of the hadronic final states produced in $p + p$, p+nucleus, and nucleus+nucleus collisions. In particular, centrality selected Pb+Pb interactions were recorded at 20A, 30A, 40A, 80A, and 158A GeV projectile energies.

The main components of the detector are four large-volume time projection chambers (TPCs), which are capable of detecting about 80% of approximately 1500 charged particles created in a central Pb+Pb collision at 158A GeV (the acceptance losses are concentrated mainly in the backward rapidity region and at azimuthal angles along the magnetic field direction). The vertex TPCs (VTPC-1 and VTPC-2), are located in the magnetic field of two superconducting dipole magnets (1.5 and 1.1 T, respectively, at 158A GeV; for lower energies, the magnetic field is scaled down in proportion to the beam energy). Two other TPCs (MTPC-L and MTPC-R) are positioned downstream of the magnets symmetrically to the beam line. The results presented in this paper are analyzed with a global tracking scheme [21], which combines track segments that belong to the same physical particle but were detected in different TPCs. The NA49 TPCs allow precise measurements of particle momenta p with a resolution of $\sigma(p)/p^2 \cong (0.3 - 7) \cdot 10^{-4}$ (GeV/c)$^{-1}$. A precise measurement of specific energy loss (dE/dx) in the region of relativistic rise is possible in the TPCs, however, dE/dx information is not used in this analysis.

The centrality of nuclear collisions is selected by using the energy of the projectile spectator nucleons measured in the downstream calorimeter (VCAL). The geometrical

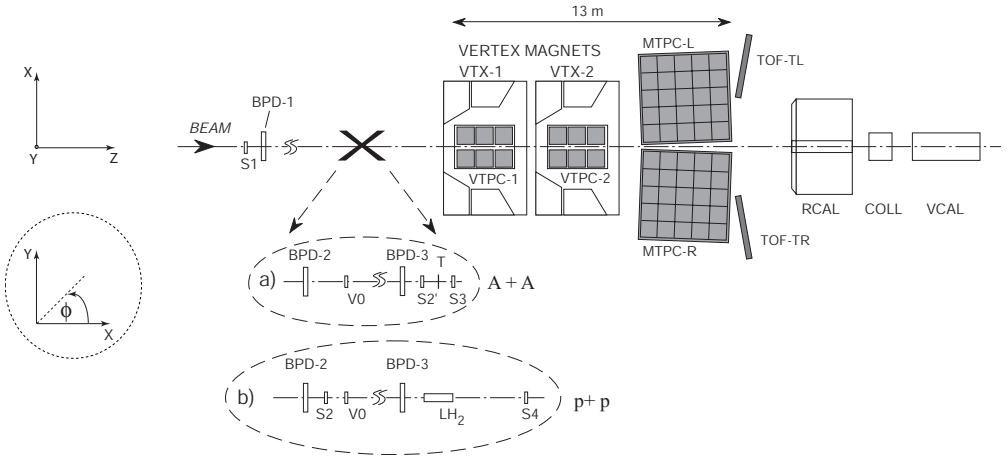

Figure 1: Experimental setup of the NA49 experiment [20] with different beam definitions and target arrangements.

acceptance of the VCAL is adjusted to cover the projectile spectator region by setting the collimator (COLL).

The target is a thin Pb foil (224 mg/cm^2) positioned about 80 cm upstream from VTPC-1. Pb beam particles are identified by means of their charge as seen by a counter (S2') situated in front of the target. The beam position detectors (BPD-1/2/3 in Fig. 1), which are proportional chambers placed along the beam line, provide a precise measurement of the transverse positions of the incoming beam particles. For Pb beams, interactions in the target are selected by an anti-coincidence of the incoming beam particle with a counter (S3) placed directly behind the target.

Details of the NA49 detector setup and performance of the tracking software are described in [20].

4 Data selection and analysis

4.1 Data sets

The data used for the analysis consist of samples of Pb+Pb collisions at 20A, 30A, 40A, 80A, and 158A GeV energy for which the 7.2% most central reactions were selected. Table 1 describes the data sets used in this analysis.

Collision energy (GeV)	Year	No. events	$\sqrt{s_{NN}}$ (GeV)	$y_{c.m.}$
20 A	2002	229 000	6.27	1.88
30 A	2002	297 000	7.62	2.08
40 A	1999	165 000	8.73	2.22
80 A	2000	228 000	12.3	2.56
158 A	1996	166 000	17.3	2.91

Table 1: Data sets used in this analysis, for 7.2% central Pb+Pb collisions: collision energy, year of data taking, number of events, center-of-mass energy $\sqrt{s_{NN}}$ for N+N pair, and center-of-mass rapidity $y_{c.m.}$ in the laboratory frame.

4.2 Event and particle selection

Event selection criteria were aimed at reducing possible contamination with nontarget collisions. The primary vertex was reconstructed by fitting the intersection point of the measured particle trajectories. Only events with a proper quality and position of the reconstructed vertex are accepted in this analysis. The vertex coordinate z along the beam has to satisfy $|z - z_0| < \Delta z$, where z_0 is the nominal vertex position and Δz is a cut parameter. The values of z_0 and Δz are -581.05 and 0.25 cm for 20A GeV, -581.3 and 0.3 cm for 30A GeV, -581.1 and 0.3 cm for 40A GeV, -581.2 and 0.3 cm for 80A GeV, and -578.9 and 0.3 cm for 158A GeV. The maximal allowed deviation of the x and y positions of the fitted vertex (Δx and Δy) from the measured beam position varies from 0.1 cm (for 158A GeV) to 0.25 cm (for low energies). The cut on the ratio of the number of tracks used to fit the primary vertex divided by the total number of tracks registered in TPCs (ntf/nto) was required to be higher than 0.25 for all energies.

To reduce the possible contamination by nonvertex tracks such as particles from secondary interactions or from weak decays, several track cuts are applied. The accepted particles are required to have measured points in at least one of the vertex TPCs. A cut on the so-called track impact parameter, the distance between the reconstructed main vertex and the back extrapolated track in the target plane $|b_x| < 2$ cm and $|b_y| < 1$ cm, is applied to reduce the contribution of nonvertex particles. Moreover, particles are accepted only when the potential number of points (nmp), calculated on the basis of the geometry of the track, in the detector exceeds 30. The ratio of the number of points on a track to the potential number of points (np/nmp) is required to be higher than 0.5 to avoid using fragments of tracks. This set of cuts significantly reduces the possible contamination of particles from weak decays, secondary interactions, and other sources.

In this analysis only tracks with $0.005 < p_T < 1.5$ GeV/c are used. For all five energies, the forward-rapidity region is selected as $1.1 < y^*_\pi < 2.6$, where y^*_π is the particle rapidity calculated in the center-of-mass reference system. As the track-by-track identification is not always possible in the experiment, the rapidities are calculated assuming the pion mass for all particles.

The NA49 detector provides a large, though incomplete, acceptance in the forward hemisphere. Figure 2 presents examples of (ϕ, p_T) acceptance [1] for $2.0 < y^*_\pi < 2.2$. The regions of complete azimuthal acceptance are different for various energies. The quantitative comparison of Φ_{p_T} values among the five energies requires selection of the regions of common acceptance.

The solid lines in Fig. 2 represent a parametrization of the common acceptance limits for all five energies by the formula -

$$p_T(\phi) = \frac{A}{\phi^2} - B, \tag{5}$$

where the parameters A and B depend on the rapidity range as given in Table 2. The same limits are used for both the negatively charged and positively charged particles with the appropriate redefinition of azimuthal angle [1]. Only particles within the acceptance limits are used in the analysis.

[1] All charged particles are plotted, with the azimuthal angle of negatively charged particles (assuming standard polarity of the magnetic field) reflected: namely for all negatively charged particles with $\phi < 0$ degrees their azimuthal angle is changed as follows: ϕ goes to ϕ+360 degrees, and finally for all negatively charged particles ϕ goes to $\phi - 180$ degrees. In the case of the opposite polarity of the magnetic field (40A GeV data) one has to redefine the azimuthal angle of positively charged particles, instead.

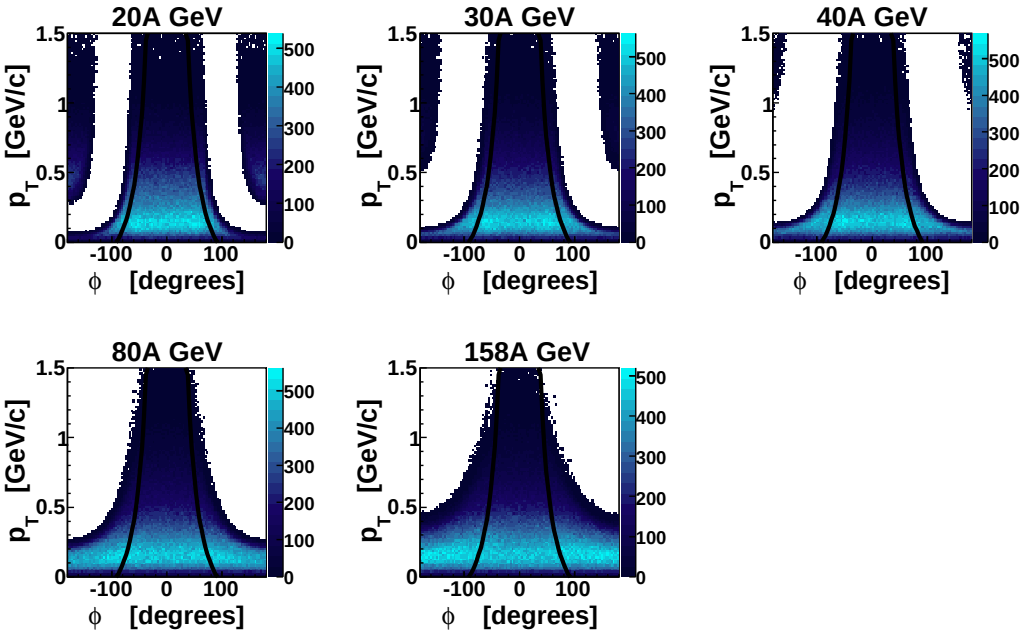

Figure 2: (Color online) NA49 (ϕ, p_T) acceptance of all charged particles for $2.0 < y^*_\pi < 2.2$. Additional cut on y^*_p (see the text) is not included. The solid lines represent the analytical parametrization of the common acceptance.

y^*_π	1.0-1.2	1.2-1.4	1.4-1.6	1.6-1.8	1.8-2.0	2.0-2.2	2.2-2.4	2.4-2.6
$A(\frac{deg.^2 GeV}{c})$	600	700	1000	2600	3000	2500	1800	1000
$B(\frac{GeV}{c})$	0.2	0.2	0.2	0.5	0.4	0.3	0.3	0.1

Table 2: Parametrization of the NA49 $\phi - p_T$ acceptance common for all five energies for positively charged particles (standard configuration of magnetic field). For negatively charged particles one has to change the definition of the azimuthal angle (see text) and then use the same parametrization.

Due to the described kinematic cuts (mostly on rapidity) and track selection criteria, together with the requirement to use the same limited (ϕ, p_T) acceptance, only about 5.0 - 5.2 % of charged particles produced in central Pb+Pb interactions (at each of the five energies) enter into the subsequent analysis.

Figure 3 presents (y^*, p_T) plots of all charged particles accepted in the analysis (additional cut on y^*_p - see below - not applied in the plots). Top, middle and bottom panels correspond to $20A$, $30A$, and $80A$ GeV data, respectively, whereas left, middle, and right panels are obtained by assuming pion, kaon and proton masses when evaluating rapidities. Black lines represent beam rapidities (y^*_{beam}) in the center-of-mass reference system. At lower energies the NA49 TPC acceptance extends to the projectile rapidity domain and the selected particles may be contaminated by e.g. elastically scattered or diffractively produced protons. This domain has been excluded from the analysis by applying an additional cut on the rapidity y^*_p of the particles, calculated with the proton mass. Namely, at each energy, the rapidity y^*_p is required to be lower than $y^*_{beam} - 0.5$.

The above cut was introduced because the preliminary analysis (without the additional y^*_p cut) manifested an unexpected effect: the Φ_{p_T} measure showed a different behavior for particles of different charges [22]. Φ_{p_T} was independent of energy and consistent with zero

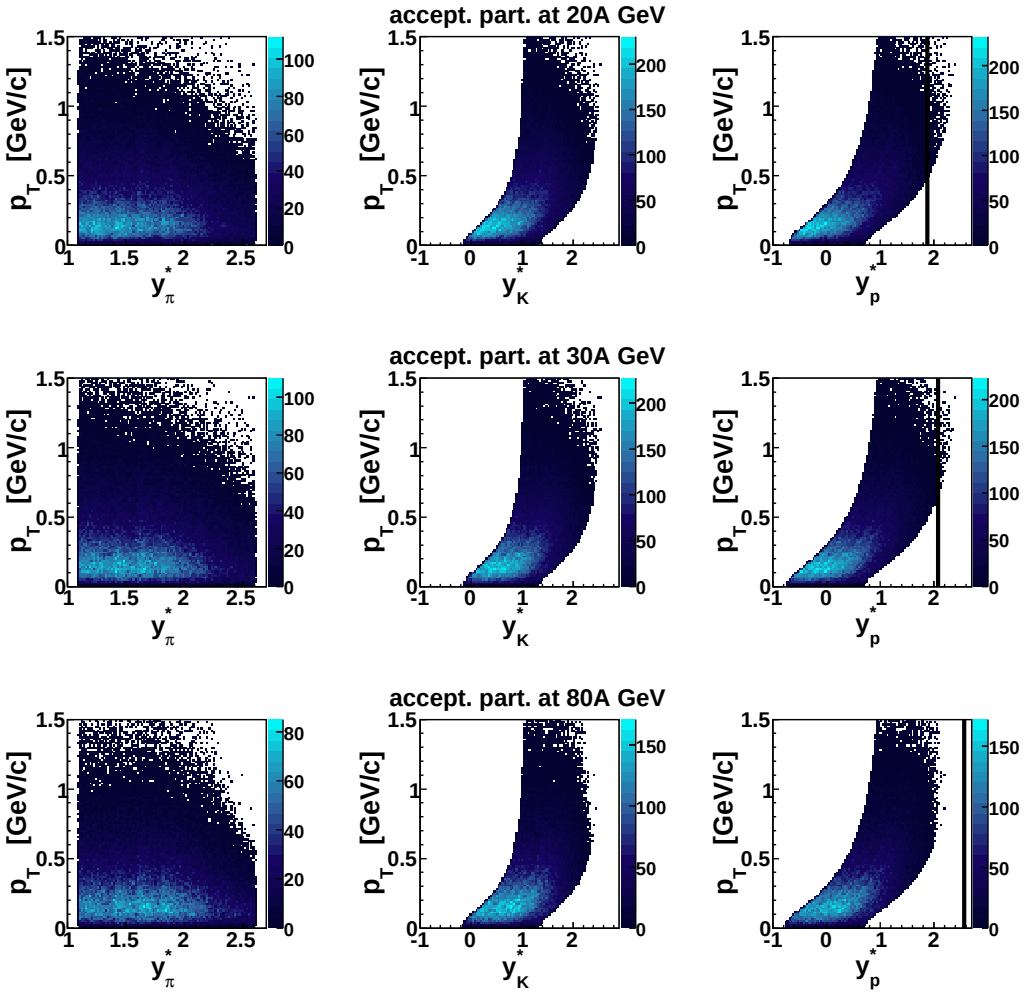

Figure 3: (Color online) (y^*, p_T) plots of all accepted (see Fig. 2) particles assuming pion (left), kaon (middle) and proton (right) mass. Additional cut on y_p^* (see the text) is not included. Top, middle, and bottom panels correspond to 20A, 30A, and 80A GeV data, respectively. Black lines represent beam rapidities (y_{beam}^*) in the center-of-mass reference system.

for negatively charged particles, but it significantly increased for lower SPS energies for both all charged and positively charged particles. This effect, however, was found to be connected with protons only, and can be explained by event-by-event impact parameter fluctuations or, more precisely, by a correlation between the number of protons (nucleons) in the forward hemisphere and the number of protons (nucleons) that are closer to the production region [23]. For more central events the number of forward-rapidity protons is smaller, and consequently, the number of protons in the production region is higher. The situation is opposite for less central collisions. The existence of those different event classes results in the increased Φ_{p_T} values for positively charged particles. One can eliminate this trivial source of correlations by either centrality restriction or rejection of the beam rapidity region [23]. In this analysis, the second method is employed by applying a cut on y_p^* at each energy (see above).

4.3 Corrections and error estimates

The statistical error on Φ_{p_T} has been estimated as follows. The whole event sample was divided into 30 independent subsamples. The value of Φ_{p_T} was evaluated for each subsample, and the dispersion - D - of the results was then calculated. The statistical error of Φ_{p_T} is taken to be equal to $D/\sqrt{30}$.

The event and track selection criteria reduce the possible systematic bias of the measured Φ_{p_T} values. To estimate the remaining systematic uncertainty, the values of cut parameters were varied within a reasonable range. For a given cut parameter, the "partial" systematic error was taken as half of the difference between the highest and the lowest Φ_{p_T} value. Two event cuts and two track cuts were considered in the analysis. The final estimate of the total systematic error on Φ_{p_T} was taken as the maximum of the changes resulting from this study.

Event cuts are used to reject possible contamination of nontarget interactions, however there is always a small fraction of remaining nontarget events that can influence the Φ_{p_T} values. This systematic bias can be estimated by investigating the dependence of Φ_{p_T} on two vertex cut parameters - ntf/nto and Δz. Figure 4 presents the dependence of Φ_{p_T} on the ratio ntf/nto for $20A$, $30A$, and $80A$ GeV data. The observed systematic error of Φ_{p_T} with respect to changes of ntf/nto varies from 0.35 MeV/c for $20A$ GeV to 0.85 MeV/c for $30A$ GeV and $80A$ GeV. In Fig. 5 the dependence of Φ_{p_T} on the allowed distance Δz from the nominal position of the main vertex is shown for three energies. The observed variation of Φ_{p_T} with this cut is quite small for all studied data sets. The highest "partial" systematic error (for $80A$ GeV data) was found to be 0.75 MeV/c.

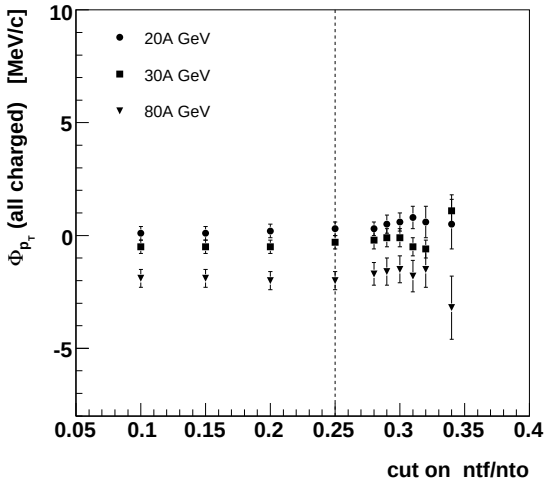

Figure 4: Dependence of Φ_{p_T} on one of the event cuts (ntf/nto ratio). Note: the values and their errors are correlated. The dashed line indicates the cut used in the analysis.

The majority of tracks selected by the track selection criteria are main vertex tracks and the remaining fraction (≈10%) originates predominantly from weak decays and secondary interactions with the material of the detector. The influence of this remaining fraction can be estimated by studying the dependence of Φ_{p_T} on the track cut parameters $|b_x|$ and $|b_y|$ and the np/nmp ratio. Figures 6 and 7 present how the values of Φ_{p_T} change with the impact parameter cut and with the cut on the np/nmp ratio, respectively. One finds that Φ_{p_T} is rather stable with respect to both cut parameters. A small increase of Φ_{p_T} with increasing impact parameter cut may be due to the increasing contribution of nonvertex tracks for higher $|b_x|$ and $|b_y|$ values. This effect has been studied quantitatively,

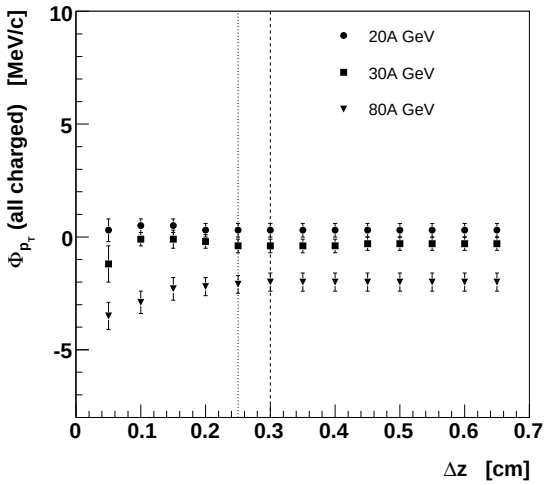

Figure 5: Dependence of Φ_{p_T} on the allowed distance Δz from the nominal position of the main vertex. Note: the values and their errors are correlated. The dashed line indicates the cut used in the analysis of 30A and 80A GeV data. The dotted line represents the cut used in the analysis of 20A GeV data.

for central Pb+Pb collisions at 158A GeV, in our previous paper [10]. The systematic error contribution from the impact parameter cut dependence varies from 0.15 MeV/c for 80A GeV to 0.55 MeV/c for 20A GeV, whereas the contribution from the change of cut in the np/nmp ratio varies from 0.45 MeV/c for 40A GeV and 80A GeV up to 1.45 MeV/c for 158A GeV.

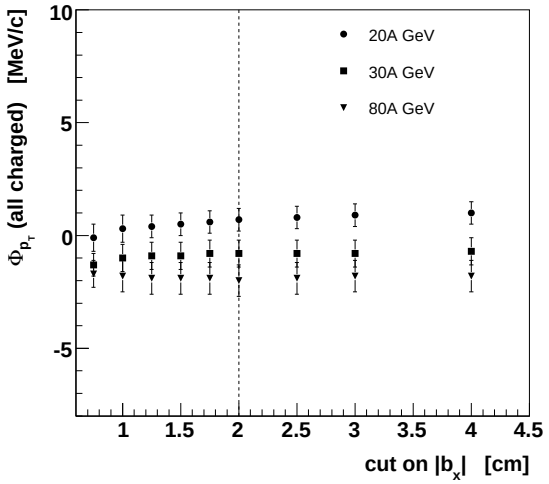

Figure 6: Dependence of Φ_{p_T} on upper cut in the impact parameter $|b_x|$. For each point, the cut on $|b_y|$ is equal to half the cut on $|b_x|$. Note: the values and their errors are correlated. The dashed line indicates the cut used in the analysis.

Finally, the typical systematic error on Φ_{p_T}, determined as the maximum resulting from the above analysis, has been estimated as not higher than 0.7 MeV/c for 20A GeV, 0.9 MeV/c for 80A GeV, 1.1 MeV/c for 40A GeV, and 1.6 MeV/c and 1.7 MeV/c for 30A and 158A GeV data, respectively. More detailed values (also for various charge selections) are given in Table 4.

The NA49 experiment registered 158A GeV Pb+Pb interactions at various beam intensities, magnetic field configurations ("normal" polarity of the magnetic field STD+

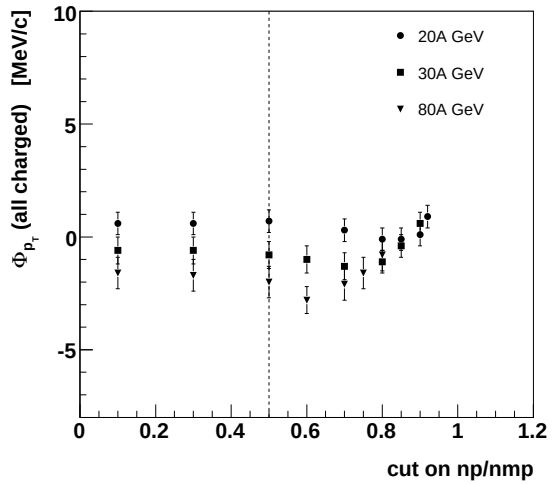

Figure 7: Dependence of Φ_{p_T} on lower cut on np/nmp ratio. Note: the values and their errors are correlated. The dashed line indicates the cut used in the analysis.

and opposite polarity of the magnetic field STD-), and with different centrality triggers. Figure 8 presents Φ_{p_T} values for these different data sets. An additional cut on the energy deposited in VCAL has been applied to select the 7.2% most central Pb+Pb interactions from each data sample. Although the numbers of events extracted from minimum-bias data are relatively low, one observes good agreement between the Φ_{p_T} values obtained for different experimental conditions.

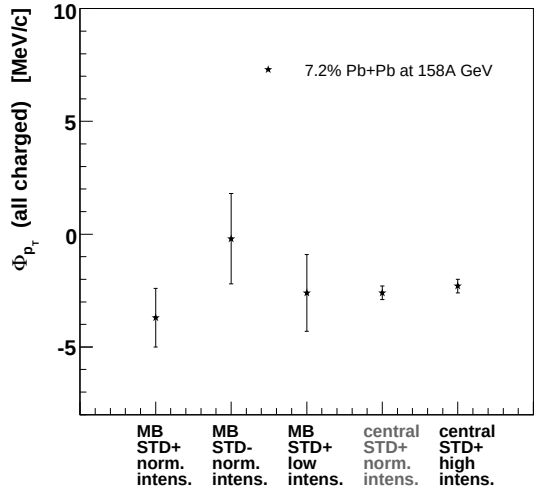

Figure 8: Φ_{p_T} values for different central and minimum-bias (MB) data sets. Data used for the further analysis are central STD+ normal intensity.

The observed Φ_{p_T} values can be affected by the losses of tracks resulting from the reconstruction inefficiency of the detector and from the track selection cuts. The dependence of Φ_{p_T} on the fraction of randomly rejected particles is shown in Fig. 9. Within the considered forward-rapidity region, at all five energies (only three example energies are shown), the tracking efficiency of the NA49 detector is higher than 95% and therefore Fig. 9 implies that the bias due to tracking inefficiency and track selection cuts is lower than 0.5 - 1.0 MeV/c.

It has already been shown in our previous paper [10] that the limited two-track resolution influences the measured Φ_{p_T} values. To quantitatively estimate this contribution,

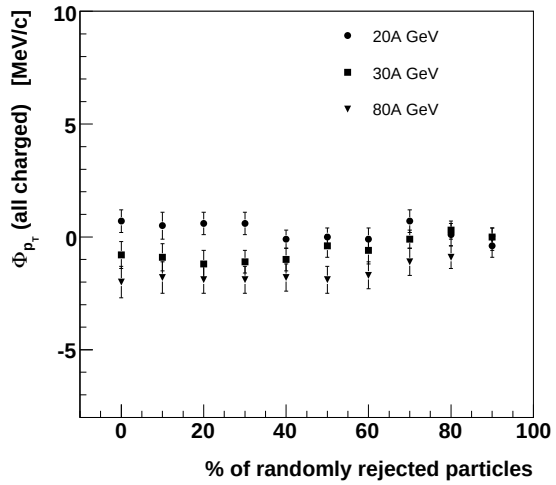

Figure 9: Dependence of Φ_{p_T} on the fraction of randomly rejected particles.

five samples (30 000 events in each) of mixed events were prepared (for 20A, 30A, 40A, 80A, and 158A GeV data). Multiplicities of mixed events were chosen to be the same as those of real events, but each particle in a mixed event was taken at random from a different real event. Such a mixing procedure ensures that the inclusive spectra (e.g., transverse momentum or rapidity) are the same for data and for mixed events, but all possible correlations vanish. Indeed, it was verified for all data sets and all particle charge selections that the Φ_{p_T} value calculated for the sample of mixed events is consistent with zero. In a second step, the prepared mixed events were processed by the NA49 simulation software. The resulting simulated raw data were then reconstructed and the Φ_{p_T} measure calculated. The obtained Φ_{p_T} values are negative, as expected for the anticorrelation introduced by the losses due to the limited two-track resolution. The additive two-track resolution correction is calculated as the difference ($\Delta\Phi_{p_T}$) between the values of Φ_{p_T} after detector simulation and reconstruction and before this procedure (mixed events). The values of $\Delta\Phi_{p_T}$ were calculated for all five energies and for various particle charge selections, separately, and are listed in Table 3.

Particles	20A	30A	40A	80A	158A
All	-0.6 ± 0.4	-0.1 ± 0.3	-0.9 ± 0.4	-1.7 ± 0.4	-3.4 ± 0.6
Negative	-0.1 ± 0.2	0.4 ± 0.2	-0.7 ± 0.3	-1.4 ± 0.2	-1.7 ± 0.5
Positive	-0.2 ± 0.4	-0.5 ± 0.4	-0.6 ± 0.4	-1.8 ± 0.5	-4.2 ± 0.7

Table 3: Values of two-track resolution corrections $\Delta\Phi_{p_T}$ (in MeV/c) for all accepted charged particles and separately for negatively and positively charged particles, for each of the five energies (in GeV).

The magnitude of the two-track resolution corrections is higher for higher energies (from 2 to 4 MeV/c for 158A GeV) where the multiplicities of produced particles are higher and consequently the densities of tracks are relatively high. The two-track resolution corrections become much smaller for low-multiplicity interactions, namely for 20A and 30A GeV data ($\Delta\Phi_{p_T}$ values close to zero). The absolute values of $\Delta\Phi_{p_T}$ are typically higher for positively than for negatively charged particles, which is mainly due to higher track density for positively charged particles caused by the larger number of protons

relative to antiprotons. The $\Delta\Phi_{p_T}$ values are typically negative thus indicating that Φ_{p_T} measured with an ideal detector would be higher. The value of Φ_{p_T} corrected for the limited two-track resolution effect equals the "raw" Φ_{p_T} minus the corresponding $\Delta\Phi_{p_T}$. The error of the corrected Φ_{p_T} is calculated by adding in squares the statistical error of the raw Φ_{p_T} value and the statistical error of the correction. As $\Delta\Phi_{p_T}$ is very small for 20A and 30A GeV data, no corrections for the two-track resolution effect were applied at these energies. Instead, the upper limits of the systematic errors were increased by 0.3 MeV/c (see Table 4).

5 Results and Discussion

5.1 Results

The results shown in this section refer to *accepted* particles, i.e., particles that are accepted by the detector and pass all kinematic cuts and track selection criteria as discussed in Sec. 4.2. Results are not corrected for limited kinematic acceptance, and this acceptance has to be taken into account when the data are compared with model predictions. The measured Φ_{p_T} values are corrected for limited two-track resolution of the NA49 detector (see below and Sec. 4.3). A possible bias due to particle losses and contamination in the accepted kinematic region is included in the systematic error.

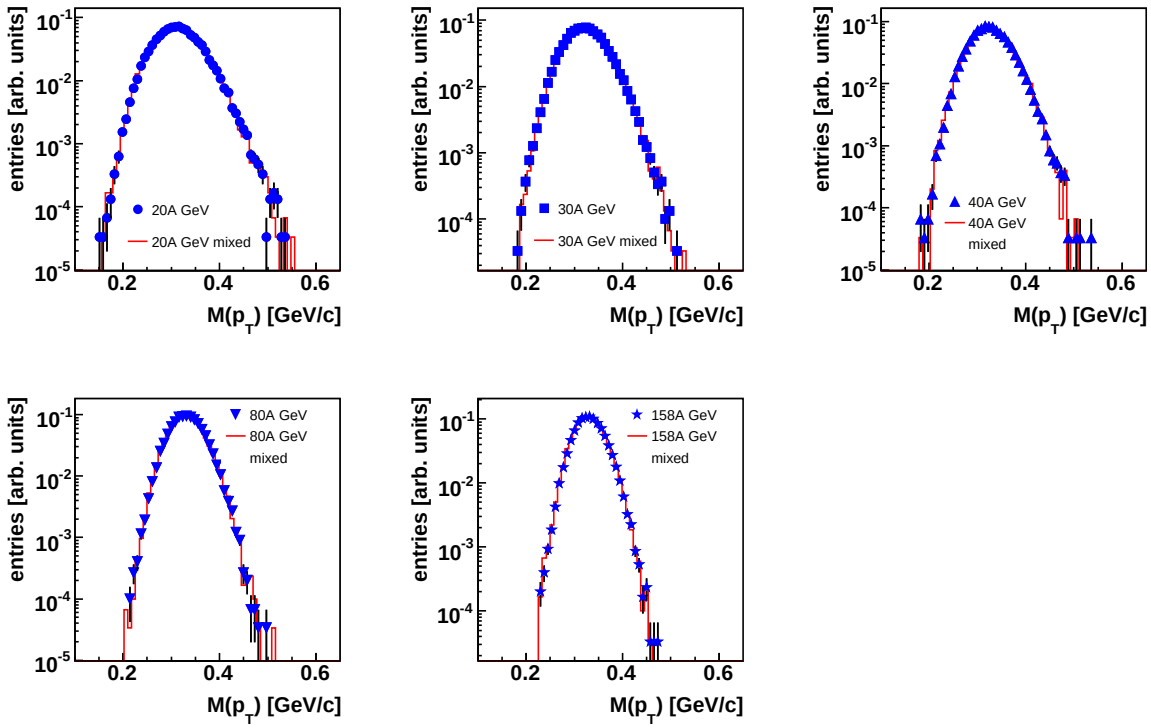

Figure 10: (Color online) Distributions of mean transverse momentum for data (points) and mixed events (histograms). Data points are not corrected for acceptance and limited two-track resolution. Events with accepted particle multiplicity equal to zero are not used.

Figure 10 shows the distributions of mean (per event) transverse momentum $M(p_T)$ for central 20A, 30A, 40A, 80A and 158A GeV Pb+Pb interactions. Points represent results from real events, and histograms are calculated from mixed events, in which there are no interparticle correlations by construction. Data are not corrected for experimental

effects such as two-track resolution or acceptance. Events with zero multiplicity (after cuts, there can be a few of them especially at lower energies) are not taken into account in Figs. 10, 11. However, when evaluating Φ_{p_T} such events are included in the data sample [2]. All charged particles are used to prepare these plots. No significant differences between the distributions of $M(p_T)$ for data and mixed events are observed at any SPS energy, indicating the absence of substantial event-by-event fluctuations. The difference between the histograms for data and mixed events can be better seen in Fig. 11, which presents the ratio of the two. At all energies, the ratio is close to unity, thus confirming that average transverse momentum fluctuations are very close to the statistical fluctuations. The widths of the distributions of $M(p_T)$ decrease with increasing energy of the colliding system as expected from the increasing particle multiplicities.

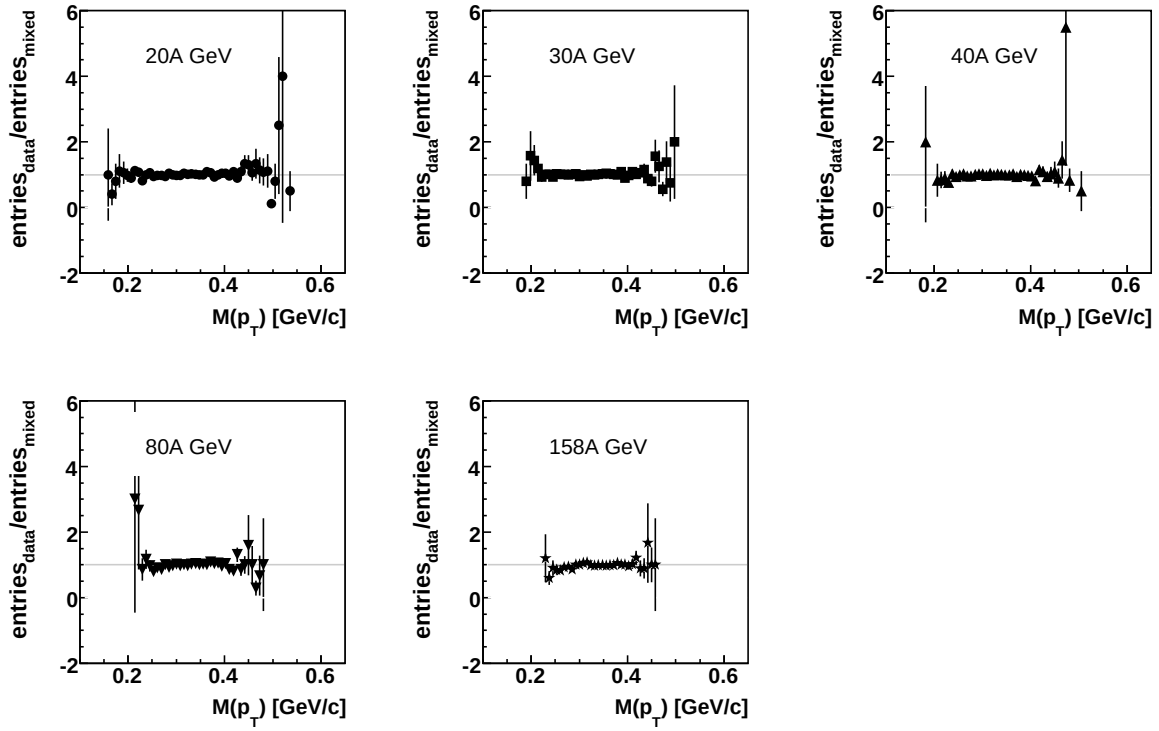

Figure 11: Distributions of mean transverse momentum for data divided by distribution for mixed events (see the previous figure).

The fluctuation measure Φ_{p_T}, which is more sensitive to small average p_T fluctuations, is shown in Fig. 12. The measured values are corrected for limited two-track resolution. Results are presented for all charged particles and separately for negatively and positively charged particles [3]. For all three charge selections, Φ_{p_T} seems to be independent of energy and consistent with the hypothesis of independent particle production ($\Phi_{p_T} \approx 0$). The

[2]It was verified that the Φ_{p_T} value does not depend on whether zero multiplicity events are included or not (in agreement with the definition of Φ_{p_T}). However, in Table 4, the mean multiplicities of accepted particles are shown, where events with zero multiplicity are normally taken into account. Thus, for consistency, the code calculating Φ_{p_T} values includes events with zero multiplicity.

[3]The sample of negatively charged particles is composed mainly of negative pions, whereas the sample of positively charged particles is dominated by positive pions and protons. Therefore, the measured fluctuations could differ between both charges. Moreover, the sample of all charged particles can include additional sources of correlations which are not present in positively or negatively charged particles, separately. Therefore the Φ_{p_T} measure obtained from all charged particles will not necessarily be a sum of Φ_{p_T} for positively and for negatively charged particles.

measured Φ_{p_T} values do not show any anomalies which might appear when approaching the phase boundary or the critical point. However, it should be noted that because of the limited acceptance of NA49 and the additional restrictions used for this analysis, the sensitivity for fluctuations may be significantly reduced if the underlying scale of the correlations is large (see Sec. 2).

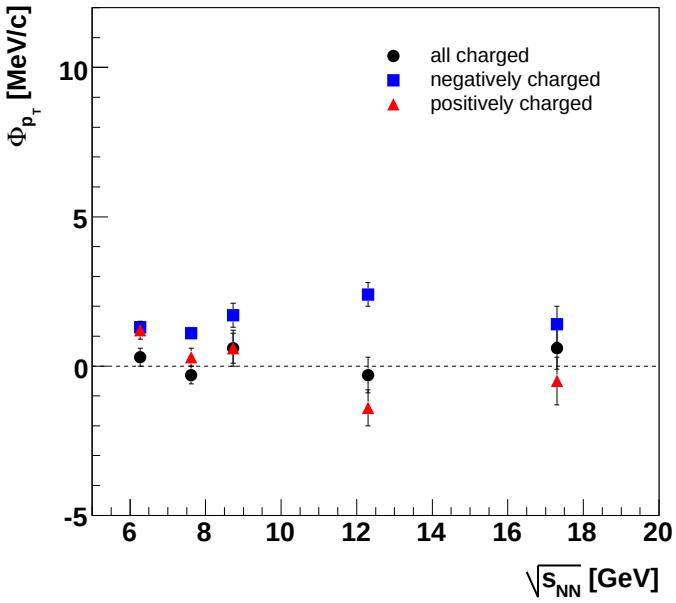

Figure 12: (Color online) Φ_{p_T} as a function of energy for the 7.2% most central Pb+Pb interactions. Data points are corrected for limited two-track resolution. Errors are statistical only. Systematic errors are given in Table 4.

Table 4 presents the mean multiplicities of accepted particles, the dispersions $\sigma_N = \sqrt{\langle N^2\rangle - \langle N\rangle^2}$ of the multiplicity distributions, the mean inclusive transverse momenta, the dispersions σ_{p_T} of inclusive transverse momentum distributions, and Φ_{p_T} values for all analyzed data sets. The Φ_{p_T} values (with their statistical and systematic errors) shown in this table have been calculated for all accepted charged particles as well as for negatively and positively charged particles, separately. All Φ_{p_T} values are corrected for the two-track resolution effect of the NA49 detector.

Energy (GeV)	$\langle N \rangle$	σ_N	$\overline{p_T}$ (MeV/c)	σ_{p_T} (MeV/c)	Φ_{p_T} ($\pm stat \pm sys$) (MeV/c)
20A (all)	29	6	314	237	$0.3 \pm 0.3\ ^{+0.9}_{-0.6}$
20A (-)	10	3	221	163	$1.3 \pm 0.2\ ^{+0.8}_{-0.5}$
20A (+)	19	4	361	254	$1.2 \pm 0.3\ ^{+1.0}_{-0.7}$
30A (all)	38	6	323	247	$-0.3 \pm 0.3\ ^{+1.3}_{-1.0}$
30A (-)	14	4	238	178	$1.1 \pm 0.2\ ^{+1.0}_{-0.7}$
30A (+)	24	5	374	267	$0.3 \pm 0.3\ ^{+1.9}_{-1.6}$
40A (all)	44	7	326	251	$0.6 \pm 0.5 \pm 0.7$
40A (-)	17	4	242	182	$1.7 \pm 0.4 \pm 0.4$
40A (+)	27	5	378	273	$0.6 \pm 0.6 \pm 1.1$
80A (all)	61	9	331	256	$-0.3 \pm 0.6 \pm 0.9$
80A (-)	26	5	270	205	$2.4 \pm 0.4 \pm 0.5$
80A (+)	35	6	378	280	$-1.4 \pm 0.6 \pm 0.9$
158A (all)	77	10	331	255	$0.6 \pm 0.7 \pm 1.5$
158A (-)	34	6	282	214	$1.4 \pm 0.6 \pm 1.0$
158A (+)	43	7	370	277	$-0.5 \pm 0.8 \pm 1.7$

Table 4: Measured inclusive and event-by-event parameters for accepted particles (results with additional y_p^* cut: see the text for more details). $\langle N \rangle$, σ_N, $\overline{p_T}$, and σ_{p_T} values are not corrected for acceptance. Φ_{p_T} values are corrected for limited two-track resolution. Φ_{p_T} values are given with statistical and systematic errors.

Two-particle correlation plots (for all charged particles) of the cumulant transverse momentum variable x are presented in Fig. 13 for 20A, 30A, 40A, 80A, and 158A GeV central Pb+Pb collisions. One observes that the plots are not uniformly populated. The color scale is the same for all plots in order to check whether the correlation pattern changes with the energy. For all five energies, short-range correlations (Bose-Einstein and Coulomb effects) are visible as an enhancement of the point density in the region close to the diagonal. The analysis of events simulated by the UrQMD model (see below) resulted in uniformly populated two-particle correlation plots without diagonal enhancement.

Figures 14 and 15 present two-particle correlation plots for different charge combinations. The correlations of both positively and negatively charged particle pairs look similar (enhancement along diagonal) and can be explained by the Bose-Einstein effect. On the other hand, there is no significant correlation observed for unlike-sign particles. The preliminary analysis for $(+-)$ pairs without azimuthal angle restrictions (see the acceptance limits in Fig. 2) showed a small maximum restricted to the region of low x (i.e. low transverse momenta) [24]. Such a low x (low p_T) maximum for unlike-sign particles was observed in the STAR data [13] and recently also by the CERES experiment [25]. This maximum was interpreted as an effect of Coulomb attraction of particles with different charges and contamination from e^+e^- pairs. When the azimuthal angle is restricted (Figs. 14 and 15) the maximum at low x is not observed any more.

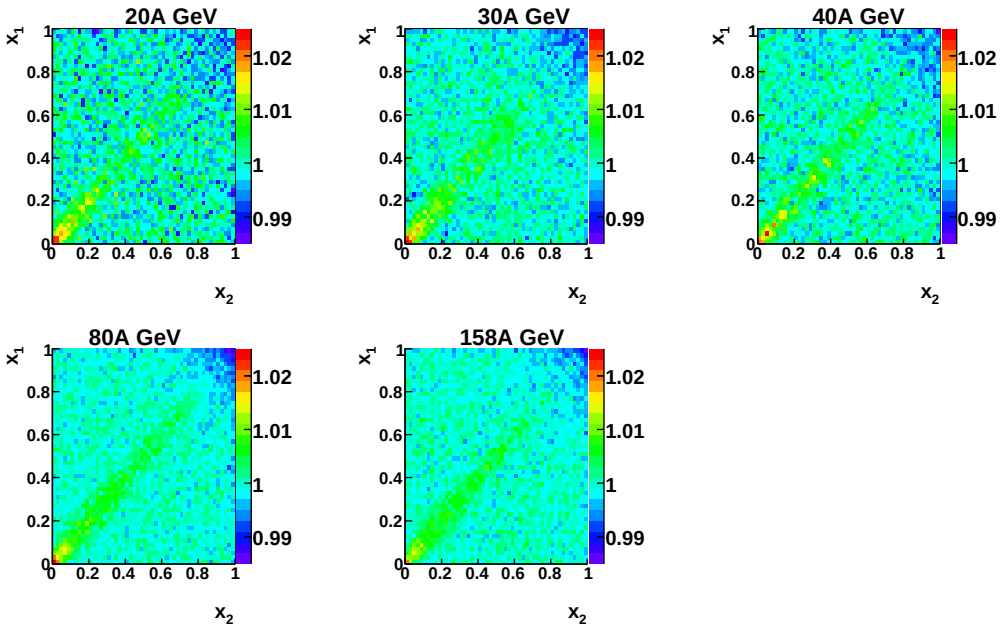

Figure 13: (Color) Two-particle correlation plots (x_1, x_2) using the cumulant p_T variable x. The bin contents are normalized by dividing with the average number of entries per bin. Plots are for all charged particles for central Pb+Pb collisions at 20A - 158A GeV. Note that the color scale is the same in all panels.

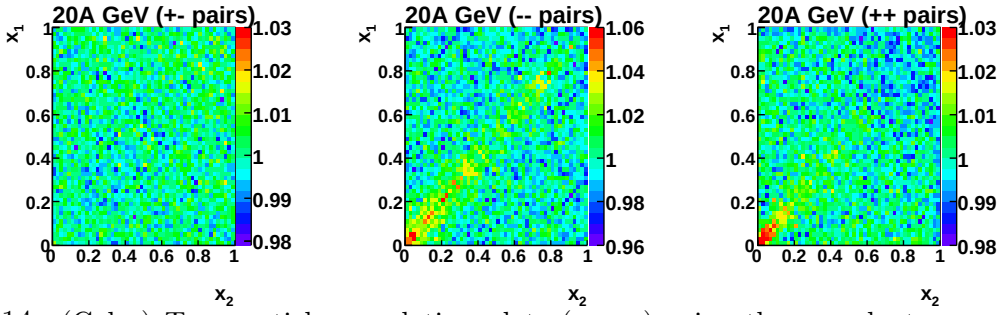

Figure 14: (Color) Two-particle correlation plots (x_1, x_2) using the cumulant p_T variable x. The bin contents are normalized by dividing with the average number of entries per bin. Plots are for central Pb+Pb collisions at 20A GeV for unlike-sign particles $(+-)$, and for negatively and positively charged particles, separately. Note that the color scale can be slightly different for different panels.

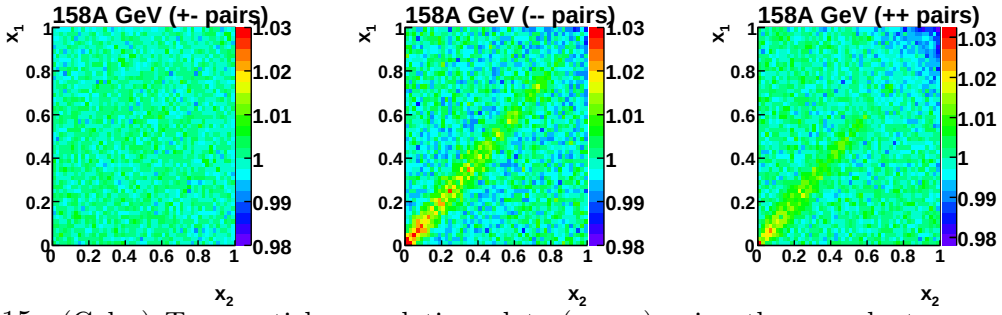

Figure 15: (Color) Two-particle correlation plots (x_1, x_2) using the cumulant p_T variable x. The bin contents are normalized by dividing with the average number of entries per bin. Plots are for central Pb+Pb collisions at 158A GeV for unlike-sign particles $(+-)$, and for negatively and positively charged particles, separately. Note that the color scale can be slightly different for different panels.

5.2 Comparison with the UrQMD model

The measured Φ_{p_T} values have been compared with the predictions of the ultrarelativistic quantum molecular dynamics (UrQMD) model [26, 27], a transport model producing hadrons via formation, decay, and rescattering of resonances and strings. In the UrQMD model, no fluctuations due to a phase transition are incorporated. However, resonance decays and effects of correlated particle production due to energy (momentum) and quantum number conservation laws are included. In the analysis default parameters of the UrQMD model were used (meson-meson and meson-baryon scattering included). For each energy the most central 7.2% interactions were selected, in accordance with the real NA49 events.

In the study of the NA49 data, the Φ_{p_T} measure was calculated from all charged particles, consistent with originating from the main vertex. This means that mostly main vertex pions, protons, kaons, and their antiparticles are used in the analysis, because particles coming from the decays of K^0_S, Λ, Ξ and Ω are suppressed by the track selection cuts. Therefore, also in the analysis of the UrQMD events only charged pions, protons and kaons were taken into account for evaluating Φ_{p_T}. Due to the specific parameter applied in the UrQMD model - the time during which all particles are tracked (taken as 80 fm/c) - the list of generated kaons, pions and (anti)protons does not contain the products of weak decays. In the analysis of the UrQMD events, the same kinematic restrictions were applied as in the case of the NA49 data. In particular, the selected (ϕ, p_T) acceptance is common for all five energies, and as a result of all the kinematic and acceptance cuts, only about 5-6% of all charged particles are used to study transverse momentum fluctuations.

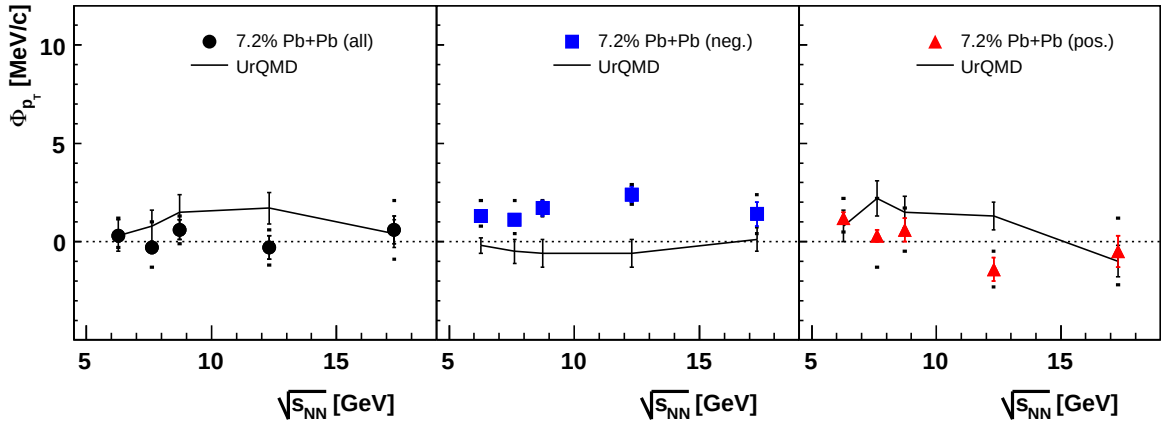

Figure 16: (Color online) Comparison of Φ_{p_T} as a function of energy from data (data points, corrected for limited two-track resolution) with UrQMD model calculations (black lines) with acceptance restrictions as for the data. The panels represent results for all charged (left), negatively charged (center) and positively charged particles (right).

Figure 16 compares the the energy dependence of Φ_{p_T} for the data and for the UrQMD model. Similar to the data, the UrQMD model does not show any significant energy dependence of transverse momentum fluctuations for any charge selection. The range of Φ_{p_T} values obtained from the UrQMD calculations is similar to that found in the data. Quantitative comparisons are not conclusive, since in spite of the same kinematic and acceptance restrictions the model does not contain the effects of Bose-Einstein correlations and Coulomb interactions. Correlations implemented in the UrQMD model (due

to conservation laws and hadron resonance production and decays) apparently do not increase the observed Φ_{p_T} values. In particular the observed differences between model and experimental data do not point to any onset of unusual fluctuations as expected for hadronic freeze-out close to the critical point.

The sensitivity of the results on the energy dependence of Φ_{p_T} to variations of the upper p_T cut was checked by repeating the analysis for three different upper p_T cuts. Figures 17, 18 and 19 show the dependence of Φ_{p_T} on energy for upper p_T cuts of 750 MeV/c, 500 MeV/c and 250 MeV/c, respectively. The measurements (data points) are corrected for limited two-track resolution. The lines represent the UrQMD predictions with the same kinematic and acceptance restrictions. The results with a decreased upper p_T cut do not show any significant energy dependence, which is similar to the corresponding results for the wide-p_T interval ($p_T < 1500$ MeV/c). The UrQMD results seem to lie systematically below the NA49 data. This effect might be explained by the neglect of Bose-Einstein and Coulomb correlations (see also Fig. 13) in the model.

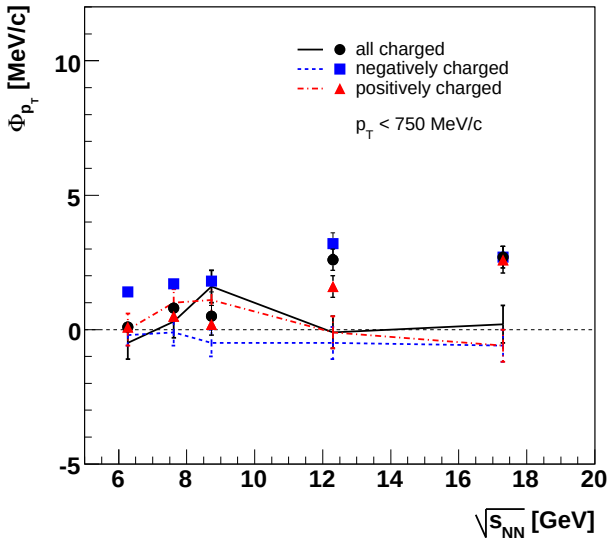

Figure 17: (Color online) Φ_{p_T} as a function of energy for the 7.2% most central Pb+Pb interactions, with additional cut $p_T < 750$ MeV/c. Data (points) are corrected for limited two-track resolution. Lines show results of UrQMD calculations with the same kinematic and acceptance restrictions. Errors are statistical only.

5.3 Search for the critical point

Recent results on the energy dependence of hadron production properties at the CERN SPS [2, 3] indicate that deconfined matter is formed at the early stage of central Pb+Pb collisions at energies as low as 30A GeV. Thus, at higher collision energies, the expanding matter crosses the phase boundary between deconfined matter and hadron gas and may freeze-out close to it. The nature of the transition is expected to change with increasing baryochemical potential μ_B. At high potential, the transition is believed to be of the first order with the end point of the first order transition line being a critical point of the second order. A characteristic property of the second-order phase transition is a divergence of the susceptibilities. Consequently, an important signal of the critical

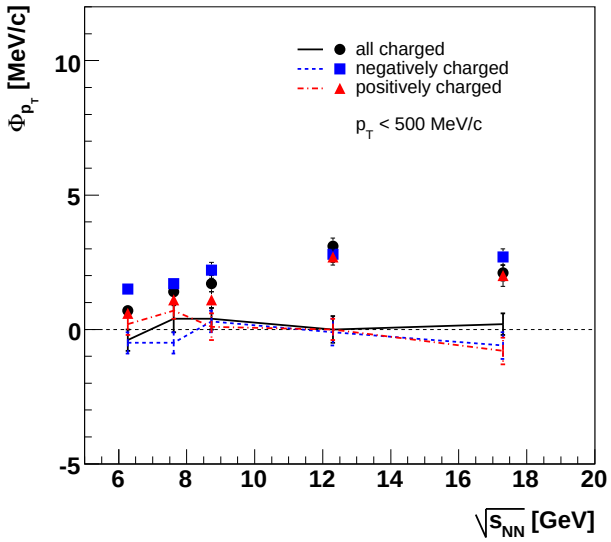

Figure 18: (Color online) Same as Fig. 17, but with additional cut $p_T < 500$ MeV/c.

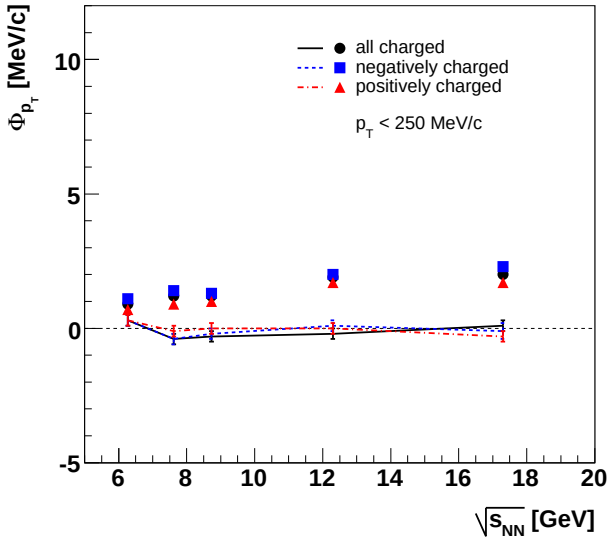

Figure 19: (Color online) Same as Fig. 17, but with additional cut $p_T < 250$ MeV/c.

point are large fluctuations, in particular, an enhancement of fluctuations of transverse momentum and multiplicity [5]. These predictions are to a large extent qualitative, as QCD at finite temperature and baryon number is one of the least accessible domains of the theory. Thus quantitative estimates of the critical point signals were performed within QCD-inspired models [5, 28, 29].

It was found that assuming a correlation length $\xi = 6$ fm and freeze-out at the critical point Φ_{p_T} in full phase space may be increased by about 40 and 20 MeV/c for all charged and for like-charge hadrons, respectively [5]. These predictions are independent of particle charge and scale with multiplicity. Therefore Φ_{p_T} for all charged hadrons is two times larger than for like-charge hadrons. The value of Φ_{p_T} is expected to decrease because of the limited acceptance, namely, by a factor of 0.6 and 0.4 for the NA49 acceptance in rapidity and in azimuthal angle, respectively. The particle correlator [5] at the critical point was calculated to be independent of azimuthal angle and charge of hadrons, whereas it changes with rapidity. Therefore the predicted Φ_{p_T} values scale with azimuthal acceptance (40%

in this analysis, independent of energy (see Fig. 2)). Together, these reduce the expected signal to about 10 and 5 MeV/c for all charged and like-charge hadrons, respectively [5] (private communication). These estimates are based on a correlation length $\xi = 6$ fm. However, because of the finite lifetime of the fireball, the correlation length may not exceed 3 fm/c [30]. Since the fluctuations scale with the square of the correlation length the expected signal is further reduced by $(6/3)^2 = 4$. This leads to estimates for Φ_{p_T} of 10 MeV/c for all charged hadrons within full phase space and about 2.4 MeV/c for all charged hadrons and 1.2 MeV/c for like-sign charged hadrons in the acceptance of the analysis. Theoretical estimates based on lattice QCD calculations locate the critical point at $T \approx 162$ MeV and $\mu_B \approx 360$ MeV [4]. Guided by the considerations of Ref. [31], we parametrize the increase of Φ_{p_T} due to the critical point by Gaussian shapes in T and μ_B with $\sigma(T) \approx 10$ MeV and $\sigma(\mu_B) \approx 30$ MeV, respectively.

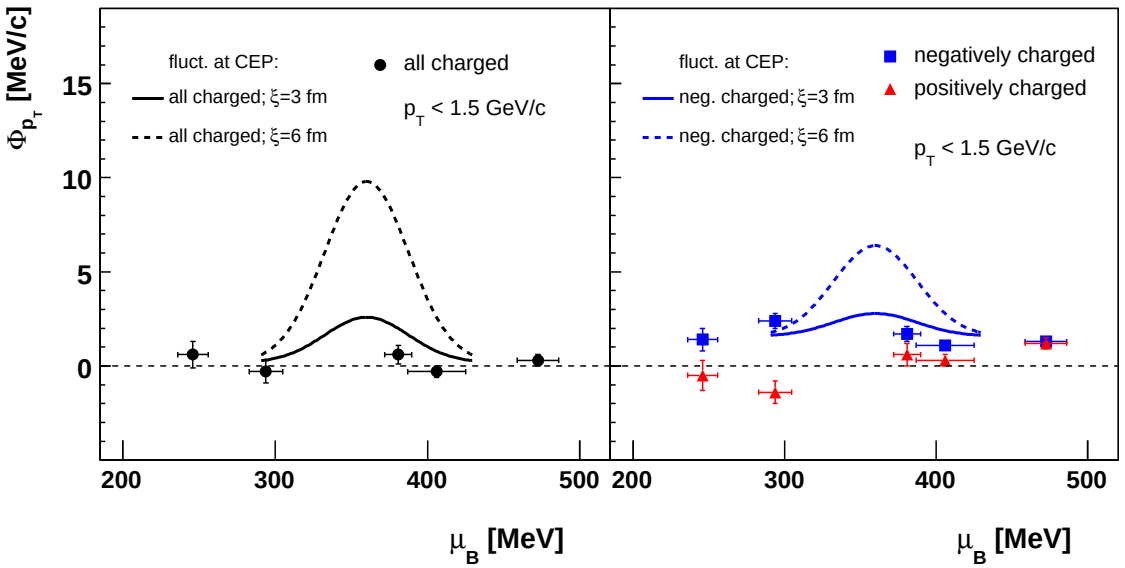

Figure 20: (Color online) Φ_{p_T} as a function of baryochemical potential (μ_B values from statistical hadron gas model fits [32]) for the 7.2% most central Pb+Pb interactions. Results with $p_T < 1.5$ GeV/c (as in Fig. 12). Data (points) are corrected for limited two-track resolution. Errors are statistical only. The Gaussian curves show estimated Φ_{p_T} values in the case of the existence of the critical point (see text for details).

The results on Φ_{p_T} in central Pb+Pb collisions at the SPS energies for $0.005 < p_T < 1.5$GeV/c and the restricted acceptance of the analysis are shown as a function of μ_B in Fig. 20. The baryochemical potential μ_B at each energy was obtained from fits of the statistical hadron gas model to the measured particle yields of NA49 [32]. The predictions for the effects of the critical point for the two assumptions on the correlation length (3 and 6 fm) are illustrated by the dashed and full Gaussian curves, respectively. The base lines of the model curves are set to the mean level of Φ_{p_T} in the SPS energy range (here the mean level is calculated separately for all charged and negatively charged particles). The data do not support the predictions for the critical point. Neither a nonmonotonic increase of Φ_{p_T} nor a characteristic difference between Φ_{p_T} for all charged and like-charge hadrons are observed. However, the freeze-out in central Pb+Pb collisions appears [32] to take place at temperatures significantly below the transition temperature and thus could make the critical point signal invisible. This possibility motivates the continuation of the search for the critical point in NA61/SHINE [33] by a scan in both temperature and baryochemical potential which will be performed by changing the collision energy and size

of the colliding nuclei.

Since publication of the NA49 results on multiplicity fluctuations [6], the estimates for the effects of the critical point have been updated. In the following, we therefore present these new predictions for multiplicity fluctuations for consistency. The estimates of the critical point signals were again performed [5] (private communication) assuming first a correlation length $\xi = 6$ fm, and they suggest an increase of the scaled variance of the multiplicity distribution ω in full phase space by 2 for all charged and by 1 for same-charge particles (uncorrelated particle production results in $\omega = 1$). The limited acceptance used in the multiplicity fluctuation analysis [6] leads to correction factors for the increase of 0.6 and 0.7 due to the rapidity and azimuthal acceptance, respectively. In the analysis of multiplicity fluctuations, the azimuthal acceptance was chosen dependent on the energy with a mean of about 70%. Thus the measured multiplicity fluctuations are expected to be increased by 0.84 and 0.42 for all charged and like-charge hadrons, respectively. For a correlation length $\xi = 3$ fm, the increase should be four times smaller, i.e., 0.5 for all charged and 0.25 for same-charge particles in full phase space and, respectively, 0.21 and 0.10 in the NA49 acceptance. Figure 21 shows the experimental results for ω as a function of baryochemical potential in the rapidity interval $1 < y^*_\pi < y^*_{beam}$ for the 1% most central Pb+Pb collisions [6]. The expectations for the critical point are represented by the Gaussian curves above base lines at the level of the mean measured values of ω. Similar to transverse momentum fluctuations, multiplicity fluctuations do not exhibit the effects expected for hadronic freeze-out close to the critical point. However, one should note that the predicted width of the critical point signal is comparable to the size of the μ_B steps in the NA49 energy scan. In future experiments, one should consider scanning with narrower steps in μ_B.

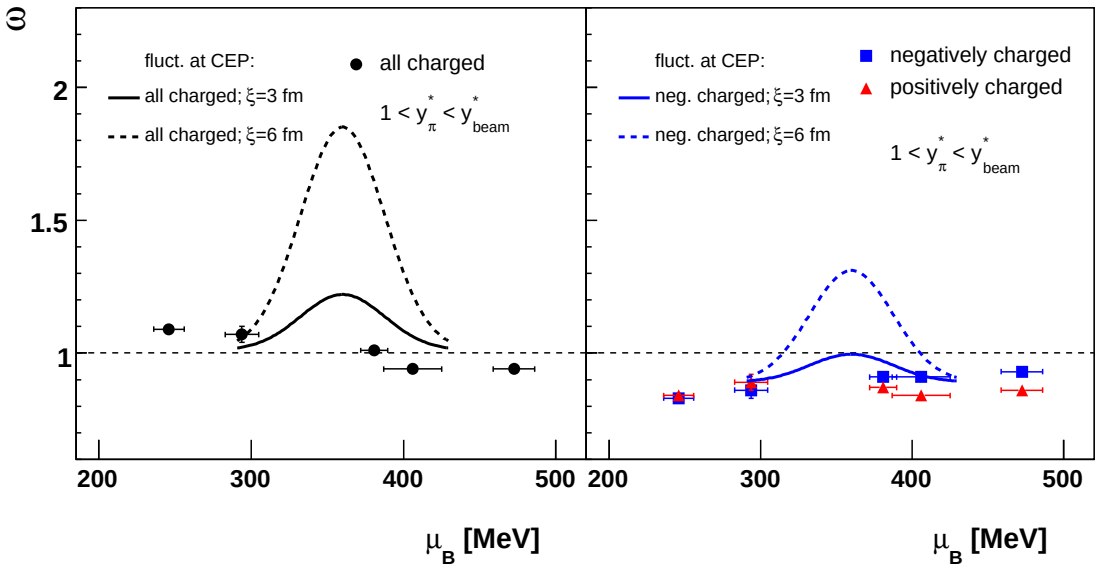

Figure 21: (Color online) ω [6] as a function of baryochemical potential (μ_B values from statistical hadron gas model fits [32]) for the 1% most central Pb+Pb interactions in $1 < y^*_\pi < y^*_{beam}$. Errors are statistical only. The Gaussian curves show estimated ω values in the case of the existence of the critical point (see text for details).

5.4 Comparison with other experiments

Event-by-event transverse momentum fluctuations have been studied by other experiments both at SPS and at RHIC energies. This section compares the NA49 results with those from the CERES and the STAR experiments. In such comparisons, one has to remember that the magnitude of any fluctuation measure may depend on the acceptance used in the analysis. The CERES experiment measured somewhat higher values of p_T fluctuations in the midrapidity region for central Pb+Au collisions at 40A, 80A, and 158A GeV. However, no significant energy dependence was found for either the $\Sigma_{p_T}(\%)$ or the Φ_{p_T} fluctuation measures [16, 34]. Figure 22 compares NA49 and CERES [16] results on the energy dependence of the Φ_{p_T} measure. One observes only very weak (if any) energy dependence of Φ_{p_T} over the whole SPS energy range. It should, however, be stressed that quantitative comparison of Φ_{p_T} values from NA49 and CERES is hampered by different acceptances (NA49: forward rapidity and limited azimuthal angle, CERES: midrapidity and complete azimuthal acceptance).

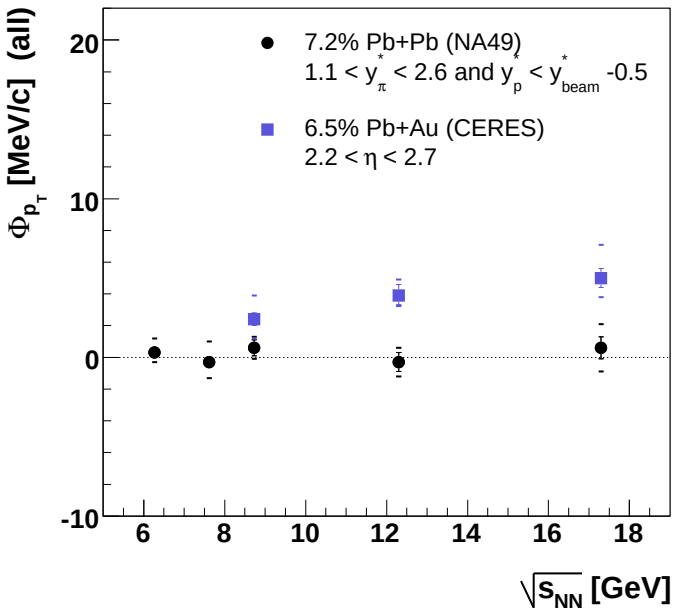

Figure 22: (Color online) Φ_{p_T} as a function of energy measured for all charged particles by the NA49 and CERES experiments. The NA49 points are obtained for the forward-rapidity region in a limited azimuthal angle acceptance; the CERES data [16] are calculated for the midrapidity region within a complete azimuthal acceptance. All data points include small-scale correlations (HBT, etc.).

The Φ_{p_T} measure is close to zero at SPS energies, but the STAR [35] results show a strong increase of Φ_{p_T} from top SPS to RHIC energies. The energy dependence of Φ_{p_T} is shown for central Pb+Pb (Pb+Au, Au+Au) collisions in Fig. 23. The data of NA49 (this paper), CERES, [16] and STAR [35] are compiled. The STAR results are presented for the related measure $\Delta\sigma_{p_T:n}$ instead of Φ_{p_T}. The difference between both measures is smaller than a few percent for high multiplicity collisions as considered here (no significant difference within the SPS energy domain and only few-percent differences at RHIC energies [35]).

The results of NA49 and CERES at $\sqrt{s_{NN}}$=17.3 GeV differ significantly from those of STAR at $\sqrt{s_{NN}}$=19.6 GeV. These differences are likely due to differences in the acceptance in momentum space. This is illustrated in Fig. 24, where Φ_{p_T} ($\Delta\sigma_{p_T:n}$) is plotted as a

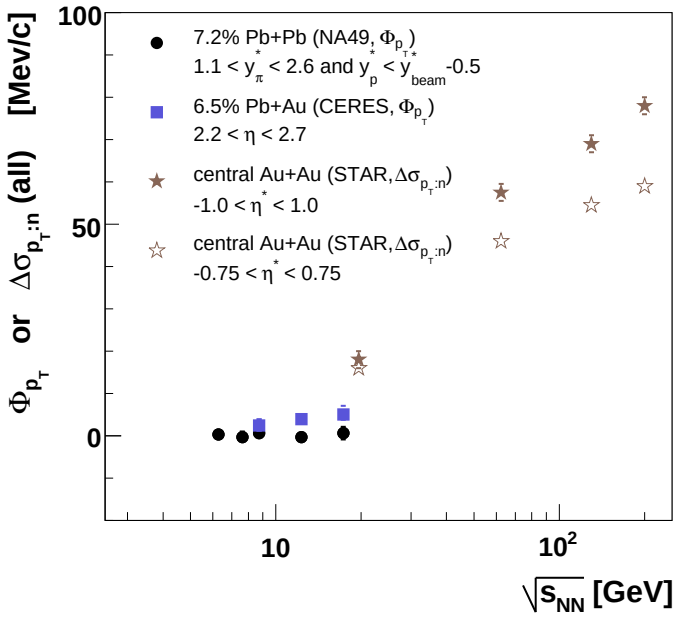

Figure 23: (Color online) Φ_{p_T} or $\Delta\sigma_{p_T:n}$ as a function of energy measured for all charged particles by the NA49, CERES, and STAR experiments. The NA49 points are obtained for the forward-rapidity region in a limited azimuthal angle acceptance; the CERES [16] and STAR (Fig. 3, left, in Ref. [35]) points are calculated for midrapidity regions within complete azimuthal acceptances. All data points include small-scale correlations (HBT, etc.). STAR data are corrected for tracking inefficiency.

function of the fraction of accepted charged particles [4]. The values of Φ_{p_T} ($\Delta\sigma_{p_T:n}$) increase with increasing fraction of accepted particles.

The striking feature of the data presented in Fig. 23 is the rapid increase of Φ_{p_T} ($\Delta\sigma_{p_T:n}$) with increasing collision energy. For a given experiment, the fraction of accepted charged particles is constant (NA49), increases (CERES), or decreases (STAR) with increasing collision energy [5]. It was already explained in Sec.2 that Φ_{p_T} is independent of acceptance changes provided the correlation scale is much smaller than the size of the acceptance region. On the other hand, when the range of correlations is significantly larger than the acceptance, Φ_{p_T} linearly decreases with decreasing fraction of accepted particles. The increase of Φ_{p_T} ($\Delta\sigma_{p_T:n}$) with energy is not caused by an increasing magnitude of short range (compared to the acceptance) correlations. As mentioned above, these correlations, if dominant, would lead to an independence of Φ_{p_T} ($\Delta\sigma_{p_T:n}$) of the acceptance, in contrast to the results shown in Fig. 24. Curiously enough, the increase of

[4]The plot shows A+A data at the top SPS energy and the lowest RHIC energy. The total multiplicities of charged particles (N_{ch}) have been obtained from the UrQMD model with centralities corresponding to the NA49, the CERES, and the STAR data. The following numbers were estimated: $N_{ch} = 1665$ for 5% most central Pb+Pb (NA49), $N_{ch} = 1567$ for 7.2% most central Pb+Pb (NA49), $N_{ch} = 1594$ for 5% most central Pb+Au (CERES), $N_{ch} = 1575$ for 6.5% most central Pb+Au (CERES), and $N_{ch} = 1401$ for 20% most central Au+Au (STAR). The values of Φ_{p_T} ($\Delta\sigma_{p_T:n}$) and multiplicities of accepted particles were taken from [10, 16, 35] and from this paper.

[5]The fraction of accepted charged particles in NA49 is about 5%, in CERES it increases from about 5.8% at 40A GeV to about 10% at 80A and 158A GeV, and for STAR this fraction decreases from about 31% at the lowest RHIC energy to approximately 17-18% at the top RHIC energy. In order to obtain the above numbers the total multiplicities of charged particles were generated within the UrQMD model with centralities corresponding to that of the NA49, the CERES, and the STAR data presented in Fig. 23. The multiplicities of *accepted* charged particles were taken from [16], [35] and from this analysis.

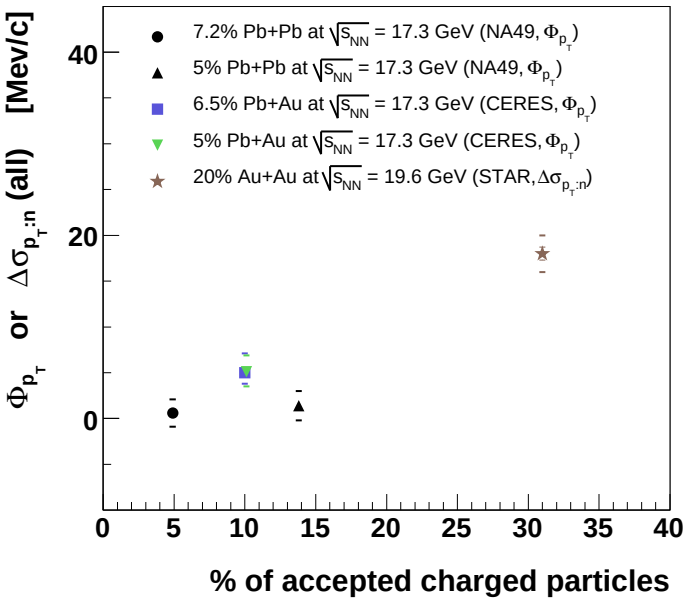

Figure 24: (Color online) Φ_{p_T} or $\Delta\sigma_{p_T:n}$ as a function of percent of charged particles accepted in the analysis. Data are presented for the top SPS and the lowest RHIC energies. The NA49 points (Ref. [10] and this analysis) are obtained for the forward-rapidity region in a limited azimuthal angle acceptance; the CERES [16] and STAR [35] points are calculated for midrapidity regions within complete azimuthal acceptances. All data points include small-scale correlations (HBT, etc.).

$\Delta\sigma_{p_T:n}$ with growing $\sqrt{s_{NN}}$ for the STAR data is associated with a decrease of the fraction of accepted particles. Consequently, we conclude that the increase is caused by a *growing* magnitude of medium- and long-range correlations (correlation length comparable to or larger than the acceptance). This effect may result from an increasing contribution of particles originating from decays of high mass resonances and/or from (mini)jet fragmentation [35].

In contrast to the Φ_{p_T} ($\Delta\sigma_{p_T:n}$) fluctuation measure, Σ_{p_T} used by the CERES experiment, does not show any dramatic differences when going from SPS to RHIC energies [16, 25] (see also Fig. 25 [6]). Also the PHENIX results confirm that the magnitude of the $\Sigma_{p_T}(\%)$ fluctuation measure exhibits only a small variation in a very wide energy range between $\sqrt{s_{NN}} = 22$ and 200 GeV [37]. It appears that the increase of Φ_{p_T} ($\Delta\sigma_{p_T:n}$) with the accepted particle multiplicity is approximately linear (Fig. 24). Consequently, $\Sigma_{p_T}(\%)$, which is proportional to $\sqrt{\Phi_{p_T}/\langle N\rangle}$, becomes approximately independent of multiplicity or collision energy.

A direct comparison of event-by-event p_T fluctuations between different experiments, based on the method of determining the magnitude of residual temperature fluctuations

[6] The NA49 Σ_{p_T} points were estimated from the values of Φ_{p_T} using the following equations: $\sigma^2_{p_T,dyn} \cong \frac{2\Phi_{p_T}\sigma_{p_T}}{\langle N\rangle}$ and finally $\Sigma_{p_T} \equiv sgn(\sigma^2_{p_T,dyn}) \cdot \frac{\sqrt{|\sigma^2_{p_T,dyn}|}}{\overline{p_T}}$ [16]. For a given $\Delta\Phi_{p_T}$ value the errors of Σ_{p_T} ($\Delta\Sigma_{p_T}{}^{upper}$ and $\Delta\Sigma_{p_T}{}^{lower}$) were calculated as: $\Delta\Sigma_{p_T}{}^{upper} = |\Sigma_{p_T}(\Phi_{p_T} + \Delta\Phi_{p_T}) - \Sigma_{p_T}(\Phi_{p_T})|$ and $\Delta\Sigma_{p_T}{}^{lower} = |\Sigma_{p_T}(\Phi_{p_T} - \Delta\Phi_{p_T}) - \Sigma_{p_T}(\Phi_{p_T})|$. Finally the NA49 $\Phi_{p_T} \pm \Delta\Phi_{p_T}$ corresponds to $\Sigma_{p_T}{}^{+\Delta\Sigma_{p_T}{}^{upper}}_{-\Delta\Sigma_{p_T}{}^{lower}}$. The same procedure was applied for statistical and systematic errors. Although the statistical and systematic errors of Φ_{p_T} are comparable at CERES and NA49, the errors of Σ_{p_T} are much higher in NA49. This is due to the fact that Σ_{p_T} is proportional to $sgn(\Phi_{p_T}) \cdot \sqrt{|\Phi_{p_T}|}$ and for Φ_{p_T} close to zero (the case of NA49) a small variation of Φ_{p_T} results in much higher changes of Σ_{p_T}.

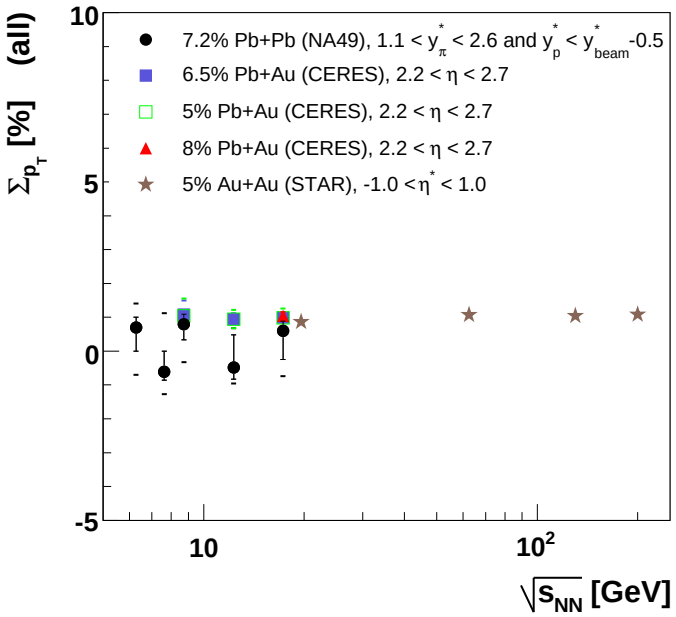

Figure 25: (Color online) $\Sigma_{p_T}(\%)$ as a function of energy measured for all charged particles by the NA49, CERES, and STAR experiments. The NA49 points are obtained for the forward-rapidity region in a limited azimuthal angle acceptance; the CERES ([16]; point for 8% most central Pb+Au collisions taken from Ref. [25]) and STAR [36] points are calculated for midrapidity regions within complete azimuthal acceptances.

[38], has been presented in Ref. [39]. For the most central interactions, the estimated temperature fluctuations are on the level of 1.8%, 1.7%, 1.3%, and 0.6% for PHENIX ($\sqrt{s_{NN}} = 200$ GeV), STAR ($\sqrt{s_{NN}} = 130$ GeV), CERES ($\sqrt{s_{NN}} = 17$ GeV), and NA49 ($\sqrt{s_{NN}} = 17$ GeV), respectively. This analysis confirms that, indeed, there is no significant energy dependence of temperature fluctuations between SPS and RHIC energies.

6 Summary and outlook

Transverse momentum event-by-event fluctuations were studied for central Pb+Pb interactions at 20A, 30A, 40A, 80A, and 158A GeV. The analysis was limited to the forward-rapidity region ($1.1 < y^*_\pi < 2.6$). Three fluctuation observables were studied: the fluctuations of average transverse momentum ($M(p_T)$) of the event, the Φ_{p_T} fluctuation measure, and transverse momentum two-particle correlations. The following results were obtained:

- The distribution of event-by-event average transverse momentum $M(p_T)$ is close to that for mixed events, indicating that fluctuations are predominantly of statistical nature.
- The fluctuation measure Φ_{p_T} has values close to zero and shows no significant energy dependence.
- Two-particle transverse momentum correlations are found to be negligible except for contributions from Bose-Einstein correlations.
- The UrQMD model reproduces the trend of the data.

- The observed smallness of p_T fluctuations in the SPS energy range is consistent with other published measurements.

- No sudden increase or nonmonotonic behavior was observed in the energy dependence of Φ_{p_T} nor the scaled variance ω of multiplicity fluctuations. Such effects have been suggested for freeze-out near the critical point of QCD.

Since the limited acceptance of NA49 is expected to reduce the signal from possible critical fluctuations, measurements in larger acceptance are still needed. Moreover, employing intermediate size nuclei may possibly move the freeze-out point closer to the critical point. These considerations motivated several new experiments planned in the SPS energy region: NA61 at the CERN SPS [40, 41, 33, 42], STAR and PHENIX at the BNL RHIC [43], MPD at the Joint Institute for Nuclear Research (JINR) Nuclotron-based Ion Collider Facility (NICA) [44], and CBM at the GSI Facility for Antiproton and Ion Research (FAIR) heavy-ion synchrotron (SIS-300) [45]. The future results, together with the existing data, will cover a broad range in the (T, μ_B) plane and should lead to significant progress in the search for the critical point.

Acknowledgments
This work was supported by the U.S. Department of Energy Grant DE-FG03-97ER41020/A000, the Bundesministerium fur Bildung und Forschung, Germany, the Virtual Institute VI-146 of Helmholtz Gemeinschaft, Germany, the Polish Ministry of Science and Higher Education (1 P03B 006 30, 1 P03B 127 30, 0297/B/H03/2007/33, N N202 078735), the Hungarian Scientific Research Foundation (T032648, T032293, T043514), the Hungarian National Science Foundation, OTKA, (F034707), the Korea Research Foundation (KRF-2007-313-C00175), the Bulgarian National Science Fund (Ph-09/05), the Croatian Ministry of Science, Education and Sport (Project 098-0982887-2878), and the Stichting FOM, the Netherlands.

References

[1] J. C. Collins and M. J. Perry, *"Superdense matter: neutrons or asymptotically free quarks?"*, Phys. Rev. Lett. **34**, 1353 (1975);
N. Itoh, *"Hydrostatic Equilibrium of Hypothetical Quark Stars"*, Prog. Theor. Phys. **44**, 291 (1970);
E. V. Shuryak, *"Quantum chromodynamics and the theory of superdense matter"*, Phys. Rept. **61**, 71 (1980);
E. V. Shuryak, *"Theory and phenomenology of the QCD vacuum"*, Phys. Rept. **115**, 151 (1984).

[2] M. Gaździcki and M. I. Gorenstein, *"On the early stage of nucleus-nucleus collisions"*, Acta Phys. Polon. **B30**, 2705 (1999).

[3] S.V. Afanasiev et al. (NA49 Collaboration), *"Energy dependence of pion and kaon production in central Pb + Pb collisions"*, Phys. Rev. **C66**, 054902 (2002).
C. Alt et al. (NA49 Collaboration), *" Pion and kaon production in central Pb + Pb collisions at 20-A and 30-A-GeV: Evidence for the onset of deconfinement"*, Phys. Rev. **C77**, 024903 (2008).

[4] Z. Fodor and S. D. Katz, *"Critical point of QCD at finite T and μ, lattice results for physical quark masses"*, JHEP **0404**, 050 (2004).

[5] M. Stephanov, K. Rajagopal, and E. V. Shuryak, *"Event-by-event fluctuations in heavy ion collisions and the QCD critical point"*, Phys. Rev. **D60**, 114028 (1999), and private communication.

[6] C. Alt et al. (NA49 Collab.), *"Energy Dependence of Multiplicity Fluctuations in Heavy Ion Collisions at the CERN SPS"*, Phys. Rev. **C78**, 034914 (2008).

[7] C. Alt et al. (NA49 Collab.), *"Electric charge fluctuations in central Pb+Pb collisions at 20, 30, 40, 80 and 158 AGeV"*, Phys. Rev. **C70**, 064903 (2004).

[8] C. Roland et al. (NA49 Collab.), *"Event-by-event fluctuations of particle ratios in central Pb+Pb collisions at 20 to 158 AGeV"*, J. Phys. **G30**, S1381 (2004).

[9] M. Gaździcki, M. I. Gorenstein and St. Mrówczyński, *"Fluctuations and Deconfinement Phase Transition in Nucleus-Nucleus Collisions"*, Phys. Lett. **B585**, 115 (2004).

[10] T. Anticic et al. (NA49 Collaboration), *"Transverse Momentum Fluctuations in Nuclear Collisions at 158 AGeV."*, Phys. Rev. **C70**, 034902 (2004).

[11] M. Bleicher et al., *"Can momentum correlations prove kinetic equilibration in heavy ion collisions at 160-A-GeV?"*, Phys. Lett. **B435**, 9 (1998);
V. P. Konchakovski, S. Haussler, M. I. Gorenstein, E. L. Bratkovskaya, M. Bleicher and H. Stöcker, *"Particle number fluctuations in high energy nucleus-nucleus collisions from microscopic transport approaches"*, Phys. Rev. **C73**, 034902 (2006);
V. P. Konchakovski, M. I. Gorenstein, E. L. Bratkovskaya and H. Stöcker, *"Baryon number and electric charge fluctuations in pb+pb collisions at SPS energies"*, Phys. Rev. **C74**, 064911 (2006);
V. P. Konchakovski, B. Lungwitz, M. I. Gorenstein and E. L. Bratkovskaya, *"Multiplicity fluctuations in nucleus-nucleus collisions: Dependence on energy and atomic number"*, Phys. Rev. **C78**, 024906 (2008).

[12] S. A. Voloshin, V. Koch and H. G. Ritter, *"Event-by-event fluctuations in collective quantities"*, Phys. Rev. **C60**, 024901 (1999).

[13] T. Trainor, *"Event-by-event analysis and the central limit theorem"*, hep-ph/0001148 (2000).

[14] K. Adox et al. (PHENIX Collab.), *"Event-by-event fluctuations in mean p_T and mean e_T in $\sqrt{s_{NN}}$ = 130 GeV Au+Au collisions"*, Phys. Rev. **C66**, 024901 (2002).

[15] R. L. Ray (for the STAR Collab.), *"Correlations, fluctuations, and flow measurements from the STAR experiment"*, Nucl. Phys. **A715**, 45 (2003).

[16] D. Adamova et al. (CERES Collab.), *"Event-by-event fluctuations of the mean transverse momentum in 40, 80, and 158 AGeV/c Pb-Au collisions"*, Nucl. Phys. **A727**, 97 (2003).

[17] S. Gavin *"Traces of Thermalization from p_t Fluctuations in Nuclear Collisions"*, Phys. Rev. Lett. **92**, 162301 (2004).

[18] M. Gaździcki and St. Mrówczyński, *"A method to study 'equilibration' in nucleus-nucleus collisions"*, Z. Phys. **C54**, 127 (1992).

[19] A. Białas and M. Gaździcki, *"A new variable to study intermittency"*, Phys. Lett. **B252**, 483 (1990).

[20] S. Afanasiev et al. (NA49 Collab.), *"The NA49 large acceptance hadron detector"*, Nucl. Instrum. Meth. **A430**, 210 (1999).

[21] L. S. Barnby et al. (NA49 Collab.), *"Reconstruction over a large rapidity interval of lambda, anti-lambda and K0(S) in the NA49 experiment"*, J. Phys. **G25**, 469 (1999).

[22] K. Grebieszkow et al. (NA49 Collab.), *"Event-by-event transverse momentum fluctuations in nuclear collisions at CERN SPS"*, PoS CPOD07 **022** (2008). (arXiv:0707.4608)

[23] K. Grebieszkow, *"Influence of Impact Parameter Fluctuations on Transverse Momentum Fluctuations"*, Phys. Rev. **C76**, 064908 (2007).

[24] K. Grebieszkow, *"On Transverse Momentum Event-by-Event Fluctuations in Nuclear Collisions at CERN SPS"*, https://edms.cern.ch/document/818514/1 (2005).

[25] D. Adamova et al. (CERES Collab.), *"Scale-dependence of transverse momentum correlations in Pb-Au collisions at 158A GeV/c"*, Nucl. Phys. **A811**, 179 (2008).

[26] S. A. Bass et al., *"Microscopic Models for Ultrarelativistic Heavy Ion Collisions"*, Prog. Part. Nucl. Phys. **41**, 225 (1998).

[27] M. Bleicher et al., *"Relativistic Hadron-Hadron Collisions and the Ultra-Relativistic Quantum Molecular Dynamics Model (UrQMD)"*, J. Phys. **G25**, 1859 (1999).

[28] F. Wilczek, *"QCD in extreme conditions"*, hep-ph/0003183 (2000);
M. A. Halasz, A. D. Jackson, R. E. Shrock, M. A. Stephanov and J. J. M. Verbaarschot, *"On the phase diagram of QCD"* Phys. Rev. **D58**, 096007 (1998);
M. Stephanov, K. Rajagopal, E. Shuryak, *"Signatures of the tricritical point in QCD"*

Phys. Rev. Lett. **81**, 4816 (1998);
J. Berges, N. Tetradis and C. Wetterich, *"Nonperturbative renormalization flow in quantum field theory and statistical physics"* Phys. Rept. **363**, 223 (2002);
M. A. Stephanov, *"QCD phase diagram and the critical point"* Prog. Theor. Phys. Suppl. **153**, 139 (2004), Int. J. Mod. Phys. **A20**, 4387 (2005) (hep-ph/0402115);
R. Casalbuoni, POS CPOD2006 **001** (2006) (hep-ph/0610179).

[29] N. G. Antoniou, Y. F. Contoyiannis, F. K. Diakonos, A. I. Karanikas, C. N. Ktorides, *"Pion production from a critical QCD phase"*, Nucl. Phys. **A693**, 799 (2001);
N. G. Antoniou, Y. F. Contoyiannis, F. K. Diakonos, G. Mavromanolakis, *"Critical QCD in nuclear collisions"*, Nucl. Phys. **A761**, 149 (2005).

[30] B. Berdnikov and K. Rajagopal, *"Slowing out-of-equilibrium near the QCD critical point"*, Phys. Rev. **D61**, 105017 (2000).

[31] Y. Hatta, T. Ikeda, *"Universality, the QCD critical / tricritical point and the quark number susceptibility"*, Phys. Rev. **D67**, 014028 (2003).

[32] F. Becattini, J. Manninen, M. Gaździcki, *" Energy and system size dependence of chemical freeze-out in relativistic nuclear collisions"*, Phys. Rev. **C73**, 044905 (2006).

[33] N. Antoniu et al. (NA49-future Collab.), *"Study of Hadron Production in Hadron-Nucleus and Nucleus-Nucleus Collisions at the CERN SPS"*, CERN-SPSC-2006-034 and SPSC-P-330 (2006).
N. Antoniu et al. (NA49-future Collab.), *"Additional Information Requested in the Proposal Review Process"*, Addendum (1) to the proposal P330, CERN-SPSC-2007-004 and SPSC-P-330 (2007).
N. Antoniu et al. (NA49-future Collab.), *"Further Information Requested in the Proposal Review Process"*, Addendum (2) to the proposal P330, CERN-SPSC-2007-019 and SPSC-P-330 (2007).

[34] D. Miśkowiec et al. (CERES Collab.), *"Collection of CERES Results"*, Nucl. Phys. **A774**, 43 (2006).

[35] J. Adams et al. (STAR Collab.), *"The energy dependence of p_t angular correlations inferred from mean-p_t fluctuation scale dependence in heavy ion collisions at the SPS and RHIC"*, J.Phys. **G33**, 451 (2007), and
Lanny Ray and Tom Trainor, private communication.

[36] J. Adams et al. (STAR Collab.), *"Incident Energy Dependence of p_T Correlations at RHIC"*, Phys. Rev. **C72**, 044902 (2005).
http://drupal.star.bnl.gov/STAR/files/starpublications/56/data.html

[37] J. T. Mitchell (for the PHENIX Collab.), *"Scaling Properties of Fluctuations and Correlation Results from PHENIX"*, J.Phys. **G34**, S911 (2007).

[38] R. Korus, St. Mrówczyński, M. Rybczyński, and Z. Włodarczyk, *"Transverse momentum fluctuations due to temperature variation in high-energy nuclear collisions"*, Phys. Rev. **C64**, 054908 (2001).

[39] J. T. Mitchell, *"An Overview of Fluctuation and Correlation Results in Relativistic Heavy Ion Collisions"*, J. Phys. **G30**, S819 (2004), and slides at the conference (Quark Matter 2004).

[40] M. Gaździcki, *"Onset of Deconfinement and Critical Point - Future Ion Program at the CERN SPS"*, nucl-ex/0512034 (2005).

[41] N. Antoniou et al., *"Letter of Intent: Study of Hadron Production in Collisions of Protons and Nuclei at the CERN SPS"*, CERN-SPSC-2006-001 and SPSC-P-329 (2006).

[42] M. Gaździcki (for the NA49-future Collab.), *"A new SPS programme"*, PoS CPOD2006 **016** (2006).

[43] G. S. F. Stephans, *"critRHIC: The RHIC Low Energy Program"*, J.Phys. **G32**, S447 (2006).
P. Sorensen (for the STAR Collab.), *"RHIC Critical Point Search: Assessing STAR's Capabilities"*, PoS CPOD2006 **019** (2006).
J. T. Mitchell (for the PHENIX Collab.), *"The PHENIX Potential in the Search for the QCD Critical Point"*, nucl-ex/0701079 (2007).

[44] A. N. Sissakian, A. S. Sorin, and V. D. Toneev, *"QCD Matter: A Search for a Mixed Quark-Hadron Phase"*, nucl-th/0608032 (2006).

[45] Proposal for an International Accelerator Facility for Research with Heavy Ions and Antiprotons, http://www.gsi.de/documents/DOC-2004-Mar-196-2.pdf (2004).
P. Senger, T. Galatyuk, D. Kresan, A. Kiseleva and E. Kryshen, PoS CPOD2006, **018** (2006).